IBRO Neuroscience Reports 18 (2025) 604–618

Contents lists available at ScienceDirect

IBRO Neuroscience Reports

journal homepage: www.sciencedirect.com/journal/IBRO-Neuroscience-Reports

Acupuncture regulates astrocyte neurotoxic polarization to protect blood–brain barrier integrity in delayed thrombolysis through mediating ERK1/2/Cx43 axis

Zhi-Hui Zhang [a,b,1], Yu Gu [c,1], Zheng Huang [a,b], Xin-Yu Liu [a,b], Wen-Tao Xu [a,b], Xin-Chang Zhang [a,b], Guang-Xia Ni [a,b,*]

[a] College of Acupuncture-Moxibustion and Tuina, Nanjing University of Chinese Medicine, Nanjing, China
[b] Key Laboratory of Acupuncture and Medicine Research of Ministry of Education, Nanjing University of Chinese Medicine, Nanjing, China
[c] State Key Laboratory of Digital Medical Engineering, School of Biological Science and Medical Engineering, Southeast University, Nanjing, China

ARTICLE INFO

Keywords:
Astrocytes
Neuroinflammation
Stroke
Thrombolysis
Acupuncture

ABSTRACT

Background: Thrombolytic therapy remains the standard treatment for acute ischemic stroke. The narrow window for thrombolysis means that delay in treatment worsens brain injury. Astrocytes regulate blood-brain barrier (BBB) integrity and neuroinflammation, yet their neurotoxic polarization exacerbates injury in neuropathological conditions, including ischemic stroke. Delayed recombinant tissue plasminogen activator (rt-PA) thrombolysis disrupts astrocyte homeostasis, further aggravating brain injury. This study investigates whether acupuncture, a key therapy in traditional Chinese medicine, alleviates delayed thrombolysis-induced injury by modulating astrocyte neurotoxic polarization and elucidates the underlying signaling pathway.

Methods: A rat model of embolic stroke with delayed rt-PA thrombolysis was established. The effects of infarct volume, BBB integrity, and neuroinflammation of acupuncture were evaluated. Bulk and single-cell transcriptomic analyses were performed to assess astrocyte-specific transcriptional changes. Western blotting, immunofluorescence, and pharmacological inhibition experiments validated molecular mechanisms.

Results: Acupuncture reduced infarct volume, improved neurological function, and restored BBB integrity. Transcriptomic analysis revealed dynamic regulation of astrocyte neurotoxic polarization following acupuncture intervention. Further validation experiments demonstrated that acupuncture suppressed the ERK1/2-Cx43 cascade, thereby attenuating astrocyte-mediated neurotoxicity. Pharmacological modulation of this pathway replicated the protective effects of acupuncture, highlighting the role in mitigating astrocyte dysfunction and promoting BBB recovery.

Conclusion: Acupuncture mitigates delayed thrombolysis-induced brain injury by modulating astrocyte polarization via the ERK1/2-Cx43 pathway. These findings highlight acupuncture as a potential strategy to enhance thrombolytic therapy safety in ischemic stroke.

1. Introduction

Stroke is a leading cause of death and disability worldwide, of which nearly 87 % are ischemic (Tsivgoulis et al., 2023). Timely intervention is critical to reopening blocked vessels, restoring blood flow to the brain, and protecting the ischemic penumbra (Campbell et al., 2019). Reperfusion using recombinant tissue-type plasminogen activator (rt-PA) remains the standard treatment (Herpich and Rincon, 2020). However, the limited therapeutic window of 4.5 hours restricts the broader application (Mendelson and Prabhakaran, 2021), and delayed thrombolytic therapy typically exacerbates ischemia reperfusion (I/R) injury. Neuroinflammation is one of the pathological processes that aggravates I/R injury (Jurcau and Simion, 2021). Following recanalization, inflammatory factors recruit more inflammatory cells, initiating an inflammatory cascade, which lead to blood-brain barrier (BBB) disruption and neuronal apoptosis, ultimately causing neurological dysfunction (Ohashi et al., 2023). Thus, developing strategies to target inflammation-related components or excessive inflammatory responses

* Corresponding author at: College of Acupuncture-Moxibustion and Tuina, Nanjing University of Chinese Medicine, Nanjing, China.
E-mail address: xgn66@njucm.edu.cn (G.-X. Ni).
[1] Joint Authors

https://doi.org/10.1016/j.ibneur.2025.04.005
Received 5 March 2025; Accepted 7 April 2025
Available online 11 April 2025

has become crucial for mitigating the damage caused by delayed rt-PA thrombolysis.

Astrocytes are the predominant cell type in the brain (Lee et al., 2022). Astrocytes surround neurons and vessels via the specialized endfeet to maintain BBB integrity. Aside from microglia, astrocytes are also crucial in regulating neuroinflammation, and thus serve as therapeutic targets in stroke (Revuelta et al., 2019). Astrocytes respond to various stimuli, including I/R, by becoming reactive and altering their gene expression profiles (Fan and Huo, 2021). Reactive astrocytes adopt a continuum of two functional states of polarization, neurotoxic astrocytes (A1 type) versus neuroprotective astrocytes (A2 types) (Liddelow and Barres, 2017). Growing evidence supports that neurotoxic astrocytes dominate as ischemia progresses over time, secreting more complement cascade components (C3) and pro-inflammatory factors (IL-1α, TNF-α, and IFN-γ), which damage neurons and destroy BBB (Zhang et al., 2021; Liddelow et al., 2017). Inhibiting neurotoxic astrocytes was observed to decrease the expression of pro-inflammatory factors, reduce neuronal apoptosis, subsequently improve the neurological function (Wang et al., 2024; Zhang et al., 2024a; Chen et al., 2024a). Therefore, selectively regulating the neurotoxic phenotypes holds promise in the formulation of novel astrocyte-based therapeutic strategies for stroke.

Connexin 43 (Cx43) is the most abundant gap junctions (GJs) protein and is widely distributed in astrocytes (Moorer and Stains, 2017). Astrocytes utilize Cx43 to form extensive networks through GJs, facilitating the exchange of ions and small signaling molecules, which is vital for synchronizing neuronal activity and maintaining homeostasis (Moorer and Stains, 2017). However, in pathological states, Cx43 mediates oxidative stress and neuroinflammatory responses (Almad et al., 2022; Liang et al., 2020). Previous studies have shown that Cx43 overexpression results in the release of inflammatory cytokines, exacerbating the neuroinflammatory response following stroke (Chen et al., 2024b). Inhibiting Cx43 alleviates cerebral I/R injury in rats, suggesting that regulating Cx43 may offer a novel strategy for the treatment of neuroinflammatory injuries (Chen et al., 2023). In addition, ERK1/2 (extracellular signal-regulated kinase 1 and 2) are critical components of the mitogen-activated protein kinase signaling pathway (Shaul and Seger, 2007). ERK1/2 is responsible for neuronal oxidative damage after cerebral ischemia and has been reported to modulate the expression and phosphorylation of Cx43 (Chen et al., 2017; Lei et al., 2019). The interaction of ERK1/2/Cx43 pathway in neurotoxic polarization of astrocytes is worth further investigation.

Acupuncture is an effective and safe therapeutic strategy for mitigating inflammation and oxidative stress. The World Health Organization recommends acupuncture as an alternative treatment following stroke (Qin et al., 2022). Among the acupoints used for treatment, Shuigou (GV26) and Neiguan (PC6) are two key points located on the Governor Vessel (GV), which help improve cerebral circulation and oxygen supply. Evidence-based research has confirmed the crucial role of these acupoints in relieving stroke symptoms (Yang et al., 2015, 2017). In addition, our previous studies demonstrated that acupuncture at the GV26 and PC6 acupoints inhibited the ERK1/2 signaling pathway, alleviated the inflammatory response, thereby mitigated BBB disruption and inhibited neuron apoptosis and pyroptosis (Liu et al., 2024; Zhang et al., 2024b, 2020). Furthermore, we observed that acupuncture inhibited astrocyte activation and improved BBB recovery by down-regulating GFAP expression (Xu et al., 2021). However, it remains unclear whether acupuncture regulates the neurotoxic polarization of astrocytes and whether inhibition of the ERK1/2/Cx43 pathway mitigates delayed rt-PA thrombolysis-induced damage.

In this study, we established the embolic stroke model in rats to investigate the mechanisms underlying acupuncture intervention in delayed rt-PA thrombolysis. Specifically, we explored how acupuncture regulates neurotoxic polarization of astrocytes, focusing on the down-regulation of the ERK1/2/Cx43 pathway, thereby alleviating brain injury. These findings are expected to provide theoretical and experimental support for the application of acupuncture in the treatment of ischemic stroke.

2. Materials and method

2.1. Animals

Adult male Sprague Dawley (SD) rats weighing 320 ± 20 g at SPF level were obtained from Beijing Weitonglihua Animal Co., Ltd. (Beijing, China; license no. SCXK (Jing): 2021–0011.) Animal experiments were performed strictly following the guidelines of the Institutional Animal Care and Use Committee of Nanjing University of Chinese Medicine (202312A034), which adhered strictly to the guidelines set by the National Institutes of Health Animal Care and Use Committee. The rats were housed with controlled temperature and humidity, following a 12 h light/dark cycle. Before performing experiments, all rats were acclimatized to the laboratory environment for at least one week.

2.2. Experimental design

The following experimental groups were established based on main purposes. (1) To determine the therapeutic effect of acupuncture on delayed thrombolysis, rats were randomly assigned to the following five groups: sham, model, 6 h rt-PA (delayed thrombolysis), 6 h rt-PA + Acu (acupuncture), and 6 h rt-PA + sham-acu (sham acupuncture). Specifically, the sham group was designed to eliminate the influence of non-pathological factors from the surgical procedure. The model group represents baseline state of stroke. The rt-PA+sham-acu group aimed to demonstrate the effect depending on the specific acupuncture protocol and not on the random insertion of the needle at points in the body. For all groups involving the rt-PA mentioned below, the treatment was administered 6 h post-stroke. (2) To determine the role of Cx43 in the transformation of neurotoxic astrocytes, rats were assigned to the following groups: Sham, rt-PA, and rt-PA + Tat-Gap19 (Cx43 inhibitor). (3) To assess the link between acupuncture-mediated inhibition of neurotoxic astrocyte polarization and the ERK1/2-Cx43 pathway, rats were assigned to the following groups: Sham, Model, rt-PA, rt-PA + Acu, rt-PA + C6 (ERK inducer), and rt-PA + Acu + C6.

2.3. Embolic stroke model establishment

In this experiment, the Middle Cerebral Artery Occlusion (MCAO) model was established and was prepared by Zhang's method, in which a blood clot was inserted into the middle cerebral artery (Zhang et al., 2015). Briefly, Firstly, to prepare the embolus, the donor rat's external carotid artery (ECA) was catheterized, and blood was collected in PE-50 tubing from aorta ventralis. After clotting for 2 h at 37°C and refrigerating for 22 h, a clot-filled segment of the tube was transferred to a PE-10 tube for aspiration and rinsing of the clot to remove red blood cells. Then, a modified PE-50 catheter connected to a syringe was used to inject the clot into the MCA. Next, anesthetized rats were fixed and then subjected to skin disinfection. After the cervical blood vessels were exposed, ligation and temporary clamping were applied to the ECA, while a partial arteriotomy was performed. The modified PE-50 tubes containing the blood clot were introduced into the ECA and progressed towards the ICA until it reached the origin of the MCA. Following a minor withdrawal, the clot was gradually infused with saline solution. The catheter was removed after 5 min.

The success of the model was confirmed based on cerebral blood flow obstruction, monitored using a laser speckle imaging system (RWD, Shenzhen, China), with successful obstruction indicated by a significant reduction in perfusion (Figure S4). At 6 h after model establishment, rt-PA (10 mg/kg; Boehringer Ingelheim, Germany) was administered through the tail vein in the rt-PA and rt-PA+Acu group.

2.4. Acupuncture treatment

In this experiment, two acupoints were selected: Shuigou (GV26) and bilateral Neiguan (PC6). Acupoint locations were based on the acupoint map of experimental animals issued by the Chinese Acupuncture Society (China Association of Acupuncture and Moxibustion, 2021). Rats in rt-PA+Acu group were treated at 2 h post MCAO model establishment.

The location of PC6 was about 3 mm proximal to the palm crease, positioned above the median nerve. Bilateral PC6 points were stimulated by inserting 3 mm vertically and applying a reducing technique with light insertion and heavy lifting, combined with twirling motions (anticlockwise with the left hand and clockwise with the right, amplitude under 90 degrees, and a frequency of 120–160 twists per minute) for 1 min. The GV26 acupoint was located at the junction of the upper 1/3 and middle 1/3 of the upper lip. After given acupuncture at PC6, the GV26 acupoint was punctured obliquely to a depth of 2–3 mm and treated with sparrow-pecking needling until the eye became wet (about 1 min). The needles were retained, and the whole treatment duration of acupuncture was 30 min.

For the sham acupuncture group, the same procedure was followed except that the treatment tools were modified. Instead of acupuncture needles, a specialized adhesive foam pad was placed over the GV26 and bilateral PC6 acupoints. A blunt needle was inserted into the foam pad at the designated acupoint locations, ensuring that the needle tip did not penetrate the skin.

2.5. Tat-Gap19 and ceramide C6 interventions

The injection protocol for Tat-Gap19 and Ceramide C6 was as follows: Tat-Gap19 (1 μg/μl, MCE, USA) and Ceramide C6 (0.5 μg/μl, SANTA, USA) were injected at a volume of 5 μl each at coordinates 1.0 mm posterior and 1.5 mm lateral from the bregma, with a depth of 4 mm. The needle was retained for 5 minutes post-injection and then slowly withdrawn over 3 minutes.

2.6. Neurological test

The Bederson scoring system is a four-point scale that grades the severity of neurological deficits based on specific behavioral observations. Rats were scored after surgery for 24 h. The scoring criteria are as follows: 0, no apparent neurological deficit; 1, contralateral forelimb flexion; 2, decreased grip of the contralateral forelimb while tail pulled; 3, spontaneous movement in all directions and contralateral circling only if pulled by tail; 4, spontaneous contralateral circling.

2.7. Corner turning test

It assesses sensorimotor asymmetry during a unilateral stroke model. The testing apparatus consists of two acrylic plates forming acute angles. When the rat reaches the corner, the whiskers are stimulated by the borders on both sides, leading the rat to turn left or right. Healthy rats typically turn left and right equally, but rats with unilateral cerebral ischemic injury preferentially turn towards the affected side. The test was conducted 24 h after modeling, over 10 trials with 30-second intervals, and the proportion of turns toward the affected side was recorded.

2.8. TTC staining

The infarct volume measurement was performed as follows. Brain tissues were rapidly extracted from anesthetized rats 24 hours after successful modeling and cut into 2 mm sections using brain matrices. The brain slices were then placed in a 2 % TTC (2,3,5-triphenyltetrazolium chloride) solution (Sigma-Aldrich, St. Louis, MO, USA) at 37°C for 15 minutes to stain viable tissue, followed by fixation in 4 % formaldehyde solution for 24 hours. Ischemic areas of the brain tissue as white, while the normal areas appear red. The stained brain slices are scanned and photographed. ImageJ image analysis software is then used to calculate the percentage of infarct volume for each group.

2.9. Hemorrhagic transformation measurement

Rats were sacrificed via transcranial perfusion 24 h after the onset of ischemia, and the tissue of the ischemic hemisphere was dissected and separated. Brain tissues were homogenized with 2 ml PBS. The homogenate is then centrifuged at 13,000 g for 30 minutes. Finally, hemoglobin levels were measured using a hemoglobin assay kit. A microplate reader was used to measure the optical density value.

2.10. H&E staining

Rats were anesthetized 24 hours after cerebral infarction and underwent transcardial perfusion with pre-chilled saline and 4 % paraformaldehyde. The brain was quickly removed and fixed in 10 % formalin for 24–48 h. After dehydration, the brain tissues were embedded in the paraffin. Paraffin-embedded tissues were sectioned into 6-μm thick slices using a microtome, placed on glass slides, and dried at 80°C for 2 h. The deparaffinized sections were stained with Hematoxylin and Eosin (H&E) following standard protocols. After staining, the tissue sections were mounted with yellow-colored pinene resins and examined for histological changes under a light microscope (Olympus, Japan) at 200x magnifications.

2.11. EB staining

Evans blue (EB) staining was used to examine BBB permeability. The stroked rats were injected with 2 % Evans blue (EB) dye (Sigma-Aldrich, St. Louis, USA) at a dose of 0.4 ml/100 g via tail vein 2 hours before sacrifice. After anesthesia, the rats underwent myocardial perfusion with cooled saline. The brain was quickly removed and separated into hemispheres. The right hemisphere was weighed and homogenized in 500 μl of formamide per 100 mg tissue, then incubated at 60°C for 24 h. The homogenate was centrifuged at 10,000 × g for 20 minutes at 4°C, and the absorbance of EB in the supernatant was measured at 620 nm using a spectrophotometer. EB concentration (μg/g) was calculated using the formula: EB concentration (μg/ml) × volume of formamide (ml) / mass of brain tissue (g). For fluorescence imaging, following perfusion, fixation, and dehydration, brain tissues were embedded in OCT and sliced into 25 μm sections. EB fluorescence in the coronal sections was visualized using a fluorescence microscope (Leica Thunder, Germany).

2.12. Transmission electron microscopy

Transmission Electron Microscopy (TEM) was utilized to examine the ultrastructural alterations of astrocytes. The brain tissue was collected from the ipsilateral hemisphere and sliced into 1 mm^3 tissue blocks, fixing them in 2.5 % glutaraldehyde overnight at 4°C, followed by secondary fixation with 1 % osmium tetroxide for 1 hour at room temperature. The samples are then washed with PBS, dehydrated through a graded alcohol series, and embedded in 812 epoxy resin. Sections of 60 nm thickness are cut, and stained with uranyl acetate and lead citrate. Transmission electron microscope was used to visualize the ultrastructural details of astrocytes within the brain tissue.

2.13. ELISA assay

The concentrations of IL-1β, IL-6, and TNF-α were determined using ELISA kits (LAPUDA, Nanjing, China) according to the manufacturer's instructions. Briefly, 96-well plates were coated with specific capture antibodies, and samples and standards were added to the wells. After incubation, biotinylated detection antibodies and HRP-conjugated

streptavidin were added. The reaction was developed with substrate, and absorbance was measured at 450 nm.

2.14. Western blot

Total proteins were extracted from the right cerebral cortex in the ischemic penumbra and quantified using a BCA kit (Beyotime, China). Equal amounts of protein were separated by 8–12 % SDS-PAGE and transferred to PVDF membranes (Millipore, USA). The membranes were blocked with 5 % non-fat milk in TBST for 1 hour at room temperature. Membranes were incubated overnight at 4°C with primary antibodies: C3 (1:1000, 21337–1-AP, Proteintech, China), GFAP (1:2000, 3670, CST, USA), Cx43 (1:1000, 83649S, CST, China), Phospho-Connexin 43 (Ser368) (1:1000, 3511, CST, USA), ERK1/2 (1:1000, 4695, CST, USA), Phospho-ERK1/2(Thr202/Tyr204) (1:2000, 4370, CST, USA), ZO-1 (1:1000, 21773–1-AP, Proteintech, China), β-actin (1:100000, AC026, Abclonal, China), β-tublin (1:5000, 30302ES20, Yeasen, China)and GAPDH (1:200000, 60004–1-Ig, Proteintech, China). After washing, membranes were incubated with horseradish peroxidase-conjugated secondary antibodies (1:10000, Yeasen, China) for 1 hour at room temperature. Chemiluminescence detection was performed using ECL reagents (Yeasen, China) and images were captured with a Fusion Edge Multi-function Imaging System (Vilber, France). The relative optical densities of the protein bands were quantified using ImageJ software.

2.15. Immunofluorescence staining

Rats were anesthetized 24 h post-surgery and perfused intracardially. Brains were fixed with 4 % PFA, cryoprotected in 30 % sucrose, and embedded in OCT. Serial coronal sections (12–14 μm) were cut using a cryostat (Leica, Germany). The sections were washed three times with PBST and blocked with 0.3 % Triton X-100 and 5 % goat serum in PBS for 1 hour at room temperature. Sections were incubated overnight at 4°C with primary antibodies: C3 (1:100, Proteintech, China), GFAP (1:500, 3670, CST, USA), Cx43 (1:500, 83649S, CST, China), Phospho-ERK1/2(Thr202/Tyr204) (1:200, 4370, CST, USA), CD31 (1:100, Invitrogen,USA), ZO-1 (1:3000, 21773–1-AP, Proteintch, China). After washing, sections were incubated with Alexa Fluor 647-conjugated goat anti-mouse (1:500) and Alexa Fluor 488-conjugated goat anti-rabbit (1:500) secondary antibodies for 1 h. Sections were mounted with DAPI-containing antifade medium and images were captured using a fluorescence microscope (Leica Thunder, Germany).

2.16. Transcriptomic analysis

The transcriptomic sequencing data were collected using the Gene Expression Omnibus database. The bulk RNA-seq dataset, GSE262257, was generated from our previous study (Zhang et al., 2024b), which consists of expression profiling from the brain tissue of 12 rats, including sham (n = 3), model (n = 3), 6 h rt-PA (n = 3), and 6 h rt-PA+Acu (n = 3). The MCAO modeling, thrombolysis, and acupuncture interventions were the same as those used in this study. Differential expression analysis was performed using the DESeq2 R package (version 1.42.1) (Love et al., 2014), and FDR$<$ 0.05 and $|\log2(\text{fold change})| > 1$ were set as the threshold for differentially expressed genes (DEGs) identification. The clusterProfiler package (version 3.14) was used to perform over-representation analysis and identify significant Gene Ontology (GO) Biological Processes (Wu et al., 2021). Gene set enrichment analysis (GSEA) was used to analyze ERK1/2 signaling pathways enrichment by the package clusterProfiler (Subramanian et al., 2005).

The single-cell RNA sequencing (scRNA-seq) dataset, GSE174574, includes expression profiling from the brain tissue of three control mice and three ischemic stroke mice, both at one day post-MCAO or sham operation (Zheng et al., 2022). The scRNA-seq data were processed using the Seurat package (version 4.4.0) (Hao et al., 2021). Cells were meticulously screened as follows: nCount_RNA $>$ 200 and percent.mt $<$ 25. Samples were integrated using the default parameters of the FindIntegrationAnchors and IntegrateData functions. Principal component analysis was used to reduce the dimensionality and tSNE projections were generated with a perplexity of 30. Cluster-specific genes were identified via the FindAllMarkers function, and the celltype label were manual annotated based on meta-information provided in the original study. The FindMarkers function was used to identify DEGs in astrocytes between sham and MCAO group.

To evaluate the neurotoxic polarization activity of astrocytes, we collected neurotoxic polarization-related signatures and constructed the neurotoxic score using the following formula:

$$S_{neurotoxic} = \frac{1}{n}\sum_{i=1}^{n} S_i$$

Where $S_i$corresponds to the activity score calculated by one of the classic algorithms: AUCell (Liu et al., 2023), UCell (Andreatta and Carmona, 2021), singscore (Bhuva et al., 2019), ssgsea (Jin et al., 2021), or AddModuleScore (Mei et al., 2023). The signature gene of neurotoxic polarization was listed in Table S2.

2.17. Statistical analysis

The statistical analyses were carried out using GraphPad Prism (version 7.0) and R software (version 4.3.0). The mean values and standard deviations were obtained from at least three independent studies. Paired comparisons between two groups were analyzed using Student's *t*-test, while comparisons involving more than two groups were analyzed using a one-way analysis of variance and Tukey's test. Statistical significance was indicated as *p $<$ 0.05, * *p $<$ 0.01, and ***p $<$ 0.001.

3. Results

3.1. Acupuncture reduced brain injury and BBB leakage induced by delayed rt-PA thrombolysis

We assessed the protective effects of acupuncture on delayed rt-PA thrombolysis using the experimental design outlined in Fig. 1A. Ischemic stroke was induced, followed by delayed rt-PA thrombolysis 6 hours post-stroke onset. Acupuncture or sham acupuncture (sham Acu) was administered 2 hours after ischemia, and all animals were sacrificed 24 hours post-ischemia for analysis. The 6-hour time point for delayed rt-PA thrombolysis was selected based on our previous findings, which demonstrated significant cerebral injury and hemorrhagic transformation within this time frame.

We first evaluated the cerebral injury caused by rt-PA thrombolysis. No signs of cerebral infarction or neurological deficits were observed in the Sham group. Compared to the Model group, the delayed rt-PA (6 h) group showed significantly increased Bederson scores, indicating severe neurological impairments. Acupuncture combined with rt-PA treatment significantly reduced Bederson scores, whereas the sham Acu group showed no significant difference compared to the rt-PA group (Fig. 1B) This finding was further supported by the corner turn test, which demonstrated improved motor coordination in the Acu group but not in the sham Acu group (Fig. 1C). Brain infarction was further assessed using TTC staining. The rt-PA (6 h) group exhibited a substantial increase in infarction volume compared to the Sham and Model groups. Acupuncture treatment markedly reduced the infarction volume, whereas no significant difference was observed in the sham Acu group (Fig. 1D and F).

To evaluate blood-brain barrier (BBB) permeability, we conducted Evans blue dye (EB) extravasation assays. Representative images (Fig. 1E) and quantitative analysis (Fig. 1G) showed that rt-PA treatment led to significant BBB disruption, evidenced by higher EB dye extravasation. Acupuncture significantly reduced BBB permeability, indicating

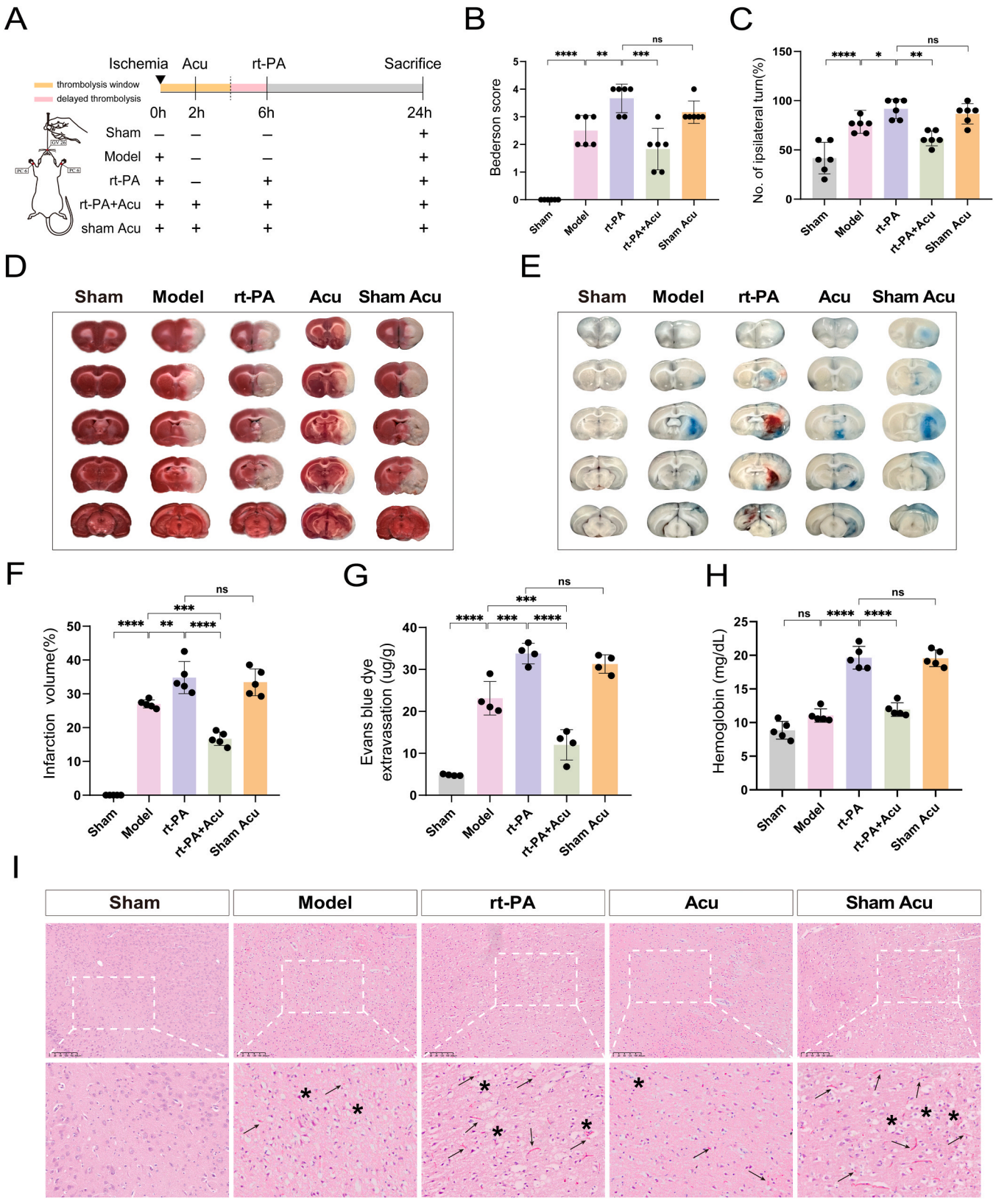

Fig. 1. Acupuncture reduced brain injury and BBB leakage induced by delayed rt-PA thrombolysis. (A) the design of experiment. (B,C) Modified Bederson score and Corner turn test results were used to assess neurological function at day 1 after modeling (n = 6). (D,E) Representative images of brain slices were stained with TTC (D) and ED dye (E) in the different experimental groups. (F) Quantification of brain infarction volume based on TTC staining (n = 5). (G) EB dye extravasation assay was used to quantify BBB permeability (n = 4). (H) Hemoglobin concentration in the ischemic hemisphere was measured by spectrophotometry, indicating hemorrhagic transformation (n = 5). (I) Representative H&E staining images (100x) was used to assess brain tissue structure of each group of rats, with arrows indicating hemorrhage and asterisks marking cellular demise. Data was presented as mean ± SD, *p < 0.05, **p < 0.01, ***p < 0.001.

improved barrier integrity. Conversely, the Sham Acu group exhibited no statistically significant improvement compared to the rt-PA group. Hemorrhagic transformation is a critical complication of rt-PA thrombolysis, which was assessed by spectrophotometric measurement of hemoglobin concentration. Hemoglobin levels were significantly elevated in the rt-PA group compared to the Sham and Model groups. Acupuncture significantly decreased hemoglobin levels, indicating reduced hemorrhagic transformation. However, the sham Acu group demonstrated no significant difference from the rt-PA group (Fig. 1H). H&E staining further illustrated extensive hemorrhagic regions (indicated by arrows) and cellular damage (marked by asterisks) in the rt-PA group, both of which were markedly alleviated by acupuncture. No observable therapeutic effect was evident in the sham Acu group (Fig. 1I). These findings indicate that acupuncture effectively lessened tissue injuries associated with ischemia and reperfusion, particularly after delayed rt-PA thrombolysis.

3.2. Transcriptomic analysis reveals dynamic regulation of astrocytes neurotoxic polarization by accupuncture intervention

Given the critical role of astrocytes in maintaining the integrity of the blood-brain barrier and their interaction with neurons (Bush et al., 1999), we focused on astrocytes for further investigation. Previous studies reported that neurological diseases induce the transformation of astrocytes into a neurotoxic A1 phenotype, which exacerbates brain injury (Zhang et al., 2022). We were curious whether the protective effect of acupuncture on delayed rt-PA thrombolysis could be related to neurotoxic polarization of astrocytes. To this end, we reanalyzed our recently published transcriptomic sequencing data, which includes the Sham, model, 6 h rt-PA, and Acupuncture + 6 h rt-PA groups. Principal component analysis revealed that, after acupuncture intervention, the distribution of the Acu group was significantly separated from that of the model and rt-PA groups (Fig. 2A). Differential expression analysis identified 1030 up-regulated and 1176 down-regulated genes. Importantly, among these genes, we find significant enrichment of the astrocytes-associated pathways (Fig. 2B). The analysis of blood brain barrier ultrastructure by electron microscopy further supported the findings. Compared to the Sham group, astrocyte endfeet exhibited swelling in the model group, which was further exacerbated in the 6 h rt-PA thrombolysis group. Acupuncture intervention effectively mitigated disruption (Fig. 2C).

Considering the masking differences in cells due to averaging in bulk sequencing, we further capture the heterogeneity of astrocytes in single-cell data. We proceeded to analyze the single-cell data from three sham-operated mice and three mice with transient middle cerebral artery occlusion operated 24 h after ischemia reperfusion (MCAO/R). After quality control, sample integration and clustering, we annotated 13 distinct cell types manually (Fig. 2D, Figure S1). By measuring gene expression of glial fibrillary acidic protein (GFAP), the astrocyte marker to index astrocytic activity, the results showed the ubiquitous expression of GFAP in the MCAO/R group, indicating the activation of astrocytes (Fig. 2E). Importantly, C3, a marker of neurotoxic astrocyte, was also highly expressed in the MCAO/R group (Fig. 2F). Further support for this conclusion is found through computational methods we refined (methods section 4.14). Higher neurotoxic polarization scores for astrocytes were observed in the MCAO/R group, confirming the occurrence of neurotoxic polarization of astrocytes following cerebral ischemia (Fig. 2G, Figure S2).

To delineate the transcriptional changes induced by neurotoxic polarization of astrocytes, we performed differential gene expression analyses. The 1379 genes in astrocytes exhibited significant changes (Fig. 2H). Among the 695 up-regulated genes, inflammatory cytokines and chemokine genes, such as Ccl4, Ccl12, Cxcl2, Ccl3, and Tnfrsf1a, were significantly upregulated, along with SerpinA3N, a gene known to promote the release of pro-inflammatory factors from neurotoxic astrocytes. The gap junction gene Cx43 was also significantly increased. Furthermore, we identified significant upregulation of matrix metalloproteinase genes MMP9 and MMP12. The elevation of MMPs has been shown to impair the neurovascular matrix and BBB integrity, leading to BBB leakage, inflammatory cell infiltration, and hemorrhagic transformation.

These transcriptomic changes align with previous studies, which documented the effects of astrocytes on the inflammatory microenvironment and the disruption of the blood-brain barrier (Bormann et al., 2024). Strikingly, among the 695 up-regulated genes, 46.4 % were significantly downregulated following acupuncture intervention in delayed thrombolytic therapy (Fig. 2I, Table S1). We further examined these transcriptomic profiles following acupuncture intervention in our data. A significant upregulation was observed after cerebral infarction and thrombolysis, which was notably reversed by acupuncture (Fig. 2J). Altogether, these results reveal transcriptomic changes associated with astrocyte neurotoxic polarization induced by delayed rt-PA thrombolysis, and demonstrate that these changes can be suppressed by acupuncture intervention.

3.3. Acupuncture inhibits neurotoxic polarization of astrocyte in delayed rt-PA thrombolysis

We sought to experimentally validate the in-silico findings. The C3 and GFAP expressions were assessed by using western blotting to examine the neurotoxic polarization of astrocytes following delayed rt-PA thrombolysis. The result showed that compared with the Sham group, C3 significantly increased in the model and 6 h rt-PA group. When rats were subjected to acupuncture, C3 expressions decreased (Fig. 3A and C). In parallel, the change trend in GFAP expression was consistent with that in C3 expression (Fig. 3B and C). We further examined the number of neurotoxic astrocytes in the ischemic penumbra using double-immunofluorescence labeling. The results showed that compared with the Sham group, the number of $C3^{+}/GFAP^{+}$ cells significantly increased in the model and 6 h rt-PA group (Fig. 3D and E). When rats were subjected to acupuncture, the number of $C3^{+}/GFAP^{+}$ cells decreased in the rt-PA+Acu group (Fig. 3D and E). These results suggest that acupuncture inhibits neurotoxic polarization of astrocytes and may reduce neuroinflammation following ischemic injury.

3.4. The expression of Cx43 associated with astrocyte neurotoxic polarization

Previous study demonstrated that Cx43, widely distributed in astrocytes, may lead to the release of inflammatory cytokines, thereby intensifying the neuroinflammatory response after stroke (Chen et al., 2023). To determine the role of Cx43 in the transformation of neurotoxic astrocytes, one group of rats were treated with the Cx43 inhibitor (Tat-Gap19) after reperfusion. Compared with the Sham group and rt-PA group, Tat-Gap19 significantly reduced the number of $GFAP^{+}$ cells (Fig. 4A and B). More importantly, Tat-Gap19 decreased C3 protein levels (Fig. 4C and D), which is consistent with the lower number of $C3^{+}/GFAP^{+}$ cells in the rt-PA-Tat-Gap19 group (Fig. 4E and F). Additionally, the increased secretion of inflammatory factors (IL-1, IL-6 and TNF-α) was abrogated after Tat-Gap19 administration (Fig. 4G-I).

We next investigated the effect of acupuncture on the expression of CX43 in neurotoxic astrocytes. Western blotting showed that compared with the Sham group, the expression of Cx43 and phosphorylated Cx43 (p-Cx43) significantly increased in both the model group and rt-PA group. Compared with those groups, Cx43 and p-Cx43 expression significantly decreased in the rt-PA+Acu group (Fig. 5A-C). The correlation analysis in protein level demonstrated that Cx43 was strongly in positive correlation with C3, and the same for pCx43 (Fig. 5D). The results of double immunofluorescence showed that the number of $Cx43^{+}/GFAP^{+}$ cells in the ischemic penumbra increased in the rt-PA group. Following the implementation of acupuncture interventions, the number of $Cx43^{+}/GFAP^{+}$ cells decreased in the rt-PA+Acu group

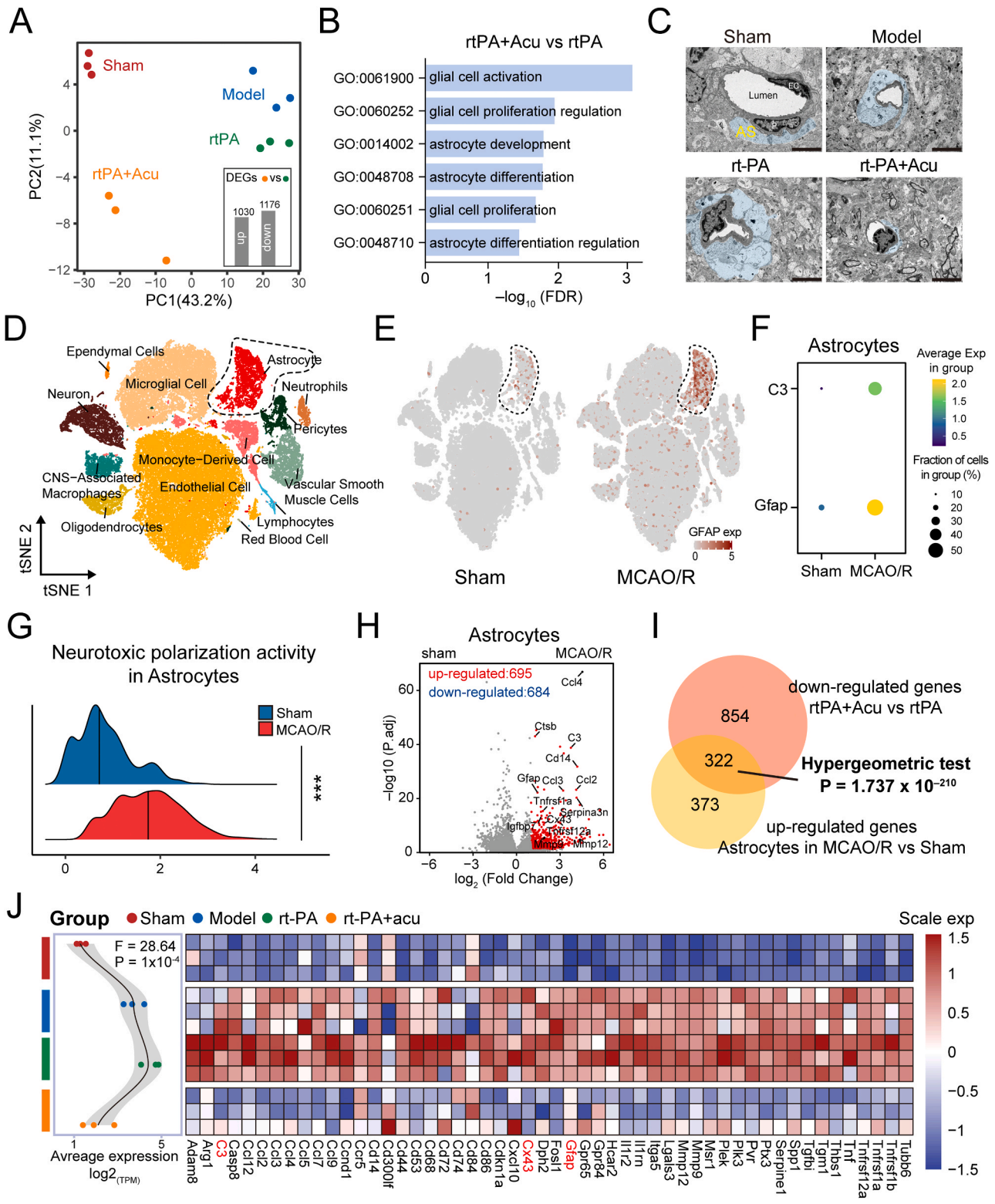

Fig. 2. Transcriptomic analysis reveals dynamic regulation of astrocytes neurotoxic polarization by accupuncture intervention. (A) Principal component analysis showing the separation between groups. The barplots in the right corner displayed the number of differentially expressed genes (DEGs) between the Acu + 6 h rt-PA vs 6 h rt-PA groups. (B) GO enrichment analysis highlighting significant astrocyte-related pathways in the Acu + 6 h rt-PA vs 6 h rt-PA comparison. (C) Electron microscopy images of astrocyte endfeet (Scale bar=2μm). (D) t-SNE clustering of single-cell data from Sham and MCAO/R groups, with 13 distinct cell types annotated. (E) tSNE plot showing higher expression of astrocyte active marker in the MCAO/R groups (F) Dotplot showing the expression of GFAP and C3. (G) Neurotoxic polarization activity scores in astrocytes from the Sham and MCAO/R groups. (H) Differential gene expression in astrocytes showing up-regulation of inflammatory and chemokine genes (Ccl4, Ccl12, Cxcl2, Ccl3, Tnfrsf1a, SerpinA3N) and the gap junction gene Cx43 in the MCAO/R group. (I) Venn diagram showing the intersection of DEGs in astrocytes of MCAO/R vs. Sham and that of Acu + 6 h rt-PA vs 6 h rt-PA groups. (J) Left: the average change in the expression of DEGs in (H). Right: The heatmap showing the expression of represent genes related to inflammatory and chemokine. Genes highlighted in red are the genes of interest. Data was presented as mean ± SD, *p < 0.05, **p < 0.01, ***p < 0.001.

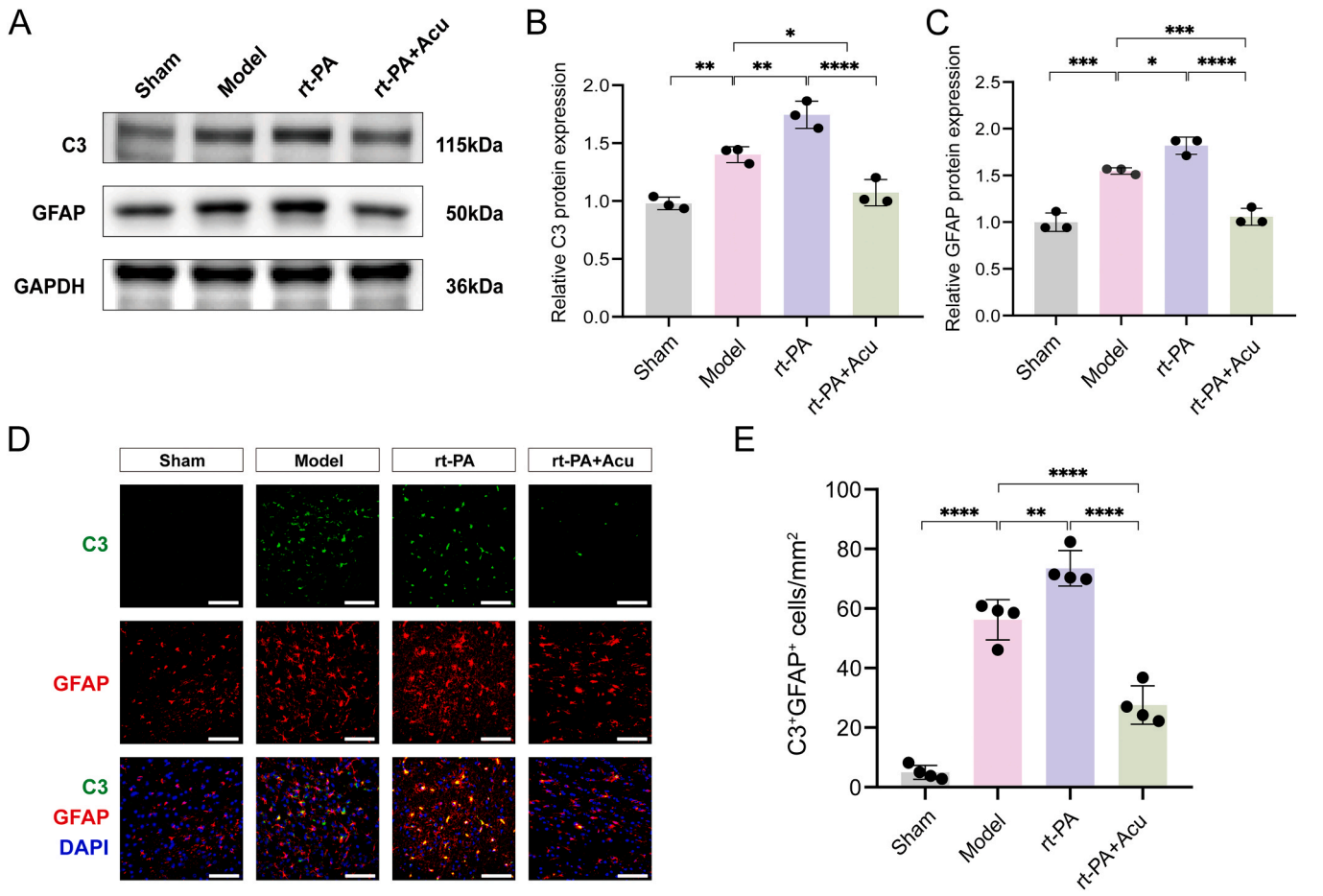

Fig. 3. Acupuncture inhibits neurotoxic polarization of astrocyte in delayed rt-PA thrombolysis. (A) Western blot analysis of C3 and GFAP expression between groups. (B, C) Quantification of C3 (B) and GFAP (C) protein expression in the western blot analysis (n = 3). (D) Double immunofluorescence staining for C3 (green) and astrocytes ($GFAP^+$ red) to detect neurotoxic astrocytes in the ischemic penumbra. (E) Quantification of neurotoxic astrocytes cells ($C3^+GFAP^+$) at 24 h after stroke in the ischemic penumbra (n = 4, Scale bar=20μm). Data was presented as mean ± SD, *p < 0.05, **p < 0.01, ***p < 0.001.

(Fig. 5E). These results revealed that the upregulation of Cx43 expressions was highly consistent with neurotoxic polarization of astrocytes, and acupuncture inhibits the expression of CX43.

3.5. *Acupuncture suppresses astrocytes neurotoxic polarization via the ERK1/2/Cx43 cascade*

Phosphorylation of Cx43 has been reported to be primarily regulated by the activation of ERK1/2 (Chen et al., 2017; Lei et al., 2019). Subsequently, we investigated whether inhibition of astrocyte neurotoxic polarization mediated by acupuncture is associated with the ERK1/2-Cx43 pathway. Gene set enrichment analysis (GSEA) was performed to evaluate significant pathway enrichment, and the ERK1/2 pathway was significantly enriched in neurotoxic polarized astrocytes (Fig. 6A). We applied the same approach using our dataset. Interestingly, the ERK1/2 pathway was significantly downregulated after acupuncture intervention in delayed reperfusion (Fig. 6B, Figure S3).

We attempted to experimentally corroborate the computational findings. We established two ERK1/2 activator groups, one received the activator (C6) after delayed reperfusion, and the other received it following delayed reperfusion with acupuncture. Following the administration of C6, p-ERK1/2 expression was markedly elevated compared to the rt-PA group, in parallel with a significant increase in p-Cx43 expression, indicating that ERK1/2 modulates Cx43 phosphorylation. Importantly, acupuncture intervention attenuated the expression of both proteins in the rt-PA and activator groups (Fig. 6C-E). The results from double immunofluorescence staining revealed a similar trend in p-ERK expression in astrocytes (Fig. 6F, G).

We further investigated the effect of the ERK1/2-Cx43 pathway on astrocyte neurotoxic polarization. Western blotting showed that, the expression of C3 increased after the administration of ERK1/2 activator, and acupuncture intervention attenuated the expression of C3 (Fig. 7A, B). Consistently, the number of $C3^+/GFAP^+$ cells increased following ERK1/2 activation and was inhibited by acupuncture (Fig. 7C, D). These results suggested that acupuncture suppresses neurotoxic polarization of astrocytes via the ERK1/2/Cx43 pathway.

3.6. *Inhibition of the ERK1/2/Cx43 pathway mitigates neuroinflammation and facilitates BBB reconstruction following delayed thrombolysis*

We determine the role of ERK1/2/Cx43 pathway in the recovery of blood brain barrier. Compared to the rt-PA group, the secretion of inflammatory factors, IL-1, IL-6 and TNF-α were increased in ERK1/2 activator group. After acupuncture intervention, these factors attenuate (Fig. 8A-C). Using Evans blue (EB) dye extravasation, we found an increase in EB fluorescence in the ischemic regions after delayed thrombolysis and C6 administration, indicating compromised blood-brain barrier integrity. However, acupuncture treatment notably reduced EB leakage (Fig. 8D).

Using immunofluorescence double labeling, tight junction protein (ZO-1) and endothelial cell (CD31) were co-stained to observe blood-brain barrier recovery. ZO-1 fluorescence intensity decreased after delayed thrombolysis and further diminished with ERK1/2 activator

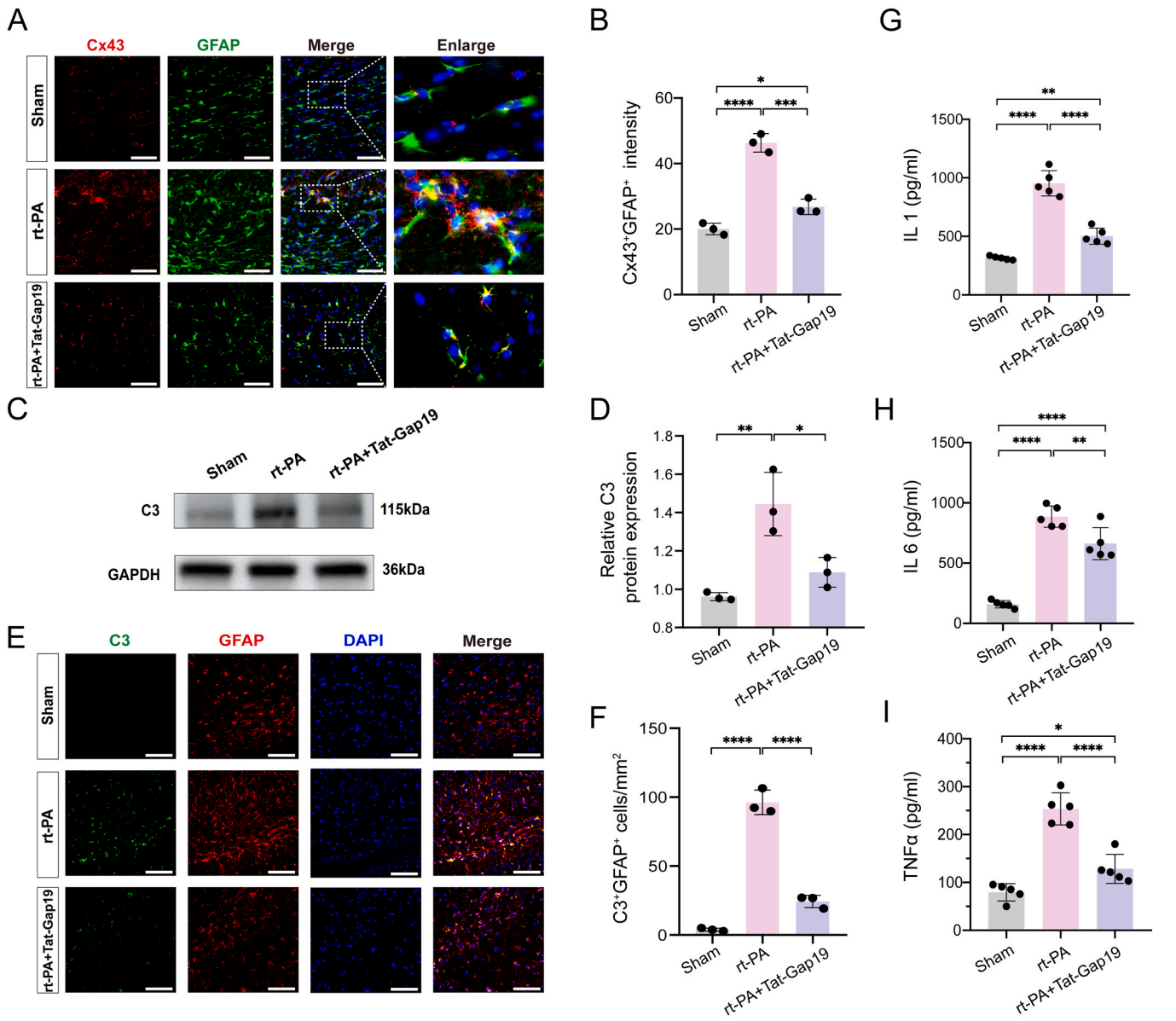

Fig. 4. Cx43 inhibition reduces neurotoxic polarization of astrocytes and inflammatory responses. (A) Representative IF images showed co-localization of Cx43 (red) and GFAP (Green) in the Sham, rt-PA, and Tat-Gap19-treated groups. (B) Quantification of $GFAP^+$ /$Cx43^+$ intensities in the brain cortex of ischemic penumbra from different groups (n = 3, Scale bar=20μm). (C) Western blot analysis of C3 expression in the groups. (D) Quantification of C3 protein expression in the western blot analysis (n = 3). (E) Double immunofluorescence staining for C3 (red) and GFAP (green) in the ischemic penumbra. (F) the number of $C3^+$/$GFAP^+$ cells were quantified in each 1 mm^2 area of the ischemic penumbra (n = 3, Scale bar=20μm). (G-I) Secretion of inflammatory cytokines IL-1β, IL-6 and TNF-α (n = 5). Data was presented as mean ± SD, *p < 0.05, **p < 0.01, ***p < 0.001.

treatment. Acupuncture intervention significantly restored fluorescence intensity, and revealed a continuous band-like morphology, indicating tight junction reconstruction in the blood-brain barrier (Fig. 8E). Further examination of ZO-1 expression supported these findings (Fig. 8F, G). Altogether, these findings suggest that acupuncture attenuates neuroinflammation and facilitates blood-brain barrier recovery through modulation of the ERK1/2/Cx43 pathway, thereby potentially mitigating brain damage beyond the therapeutic window for thrombolysis.

4. Discussion

In this study, we assessed the therapeutic efficacy of acupuncture on delayed thrombolysis. We found that acupuncture significantly reduced brain infarct volume and improved neurological function. More importantly, acupuncture decreased BBB permeability, alleviating hemorrhagic transformation. These beneficial effects were mediated through the inhibition of astrocyte neurotoxic polarization-associated inflammation, primarily via the suppression of the ERK1/2/Cx43 signaling pathway.

Acupuncture is a therapeutic modality guided by Traditional Chinese Medicine's meridian theory, which stimulates the energetic activity of acupoints. A growing amount of evidence supports the beneficial effects of acupuncture treatment for neurological function impairment in post-stroke patients. Shuigou (GV26) and Neiguan (PC6) are acupoints in classic acupuncture method, namely Xingnao Kaiqiao, selected for roles in promoting the flow of Qi and blood to the brain, improving vascular regulation, and enhancing cerebral blood flow and oxygen supply. In this study, we observed that the combination of acupuncture and rt-PA thrombolysis not only significantly reduced the neurological deficit score and brain infarction volume, but also effectively mitigated hemorrhagic transformation and tissue damage following delayed thrombolysis for 6 hours. These findings provide experimental evidence for

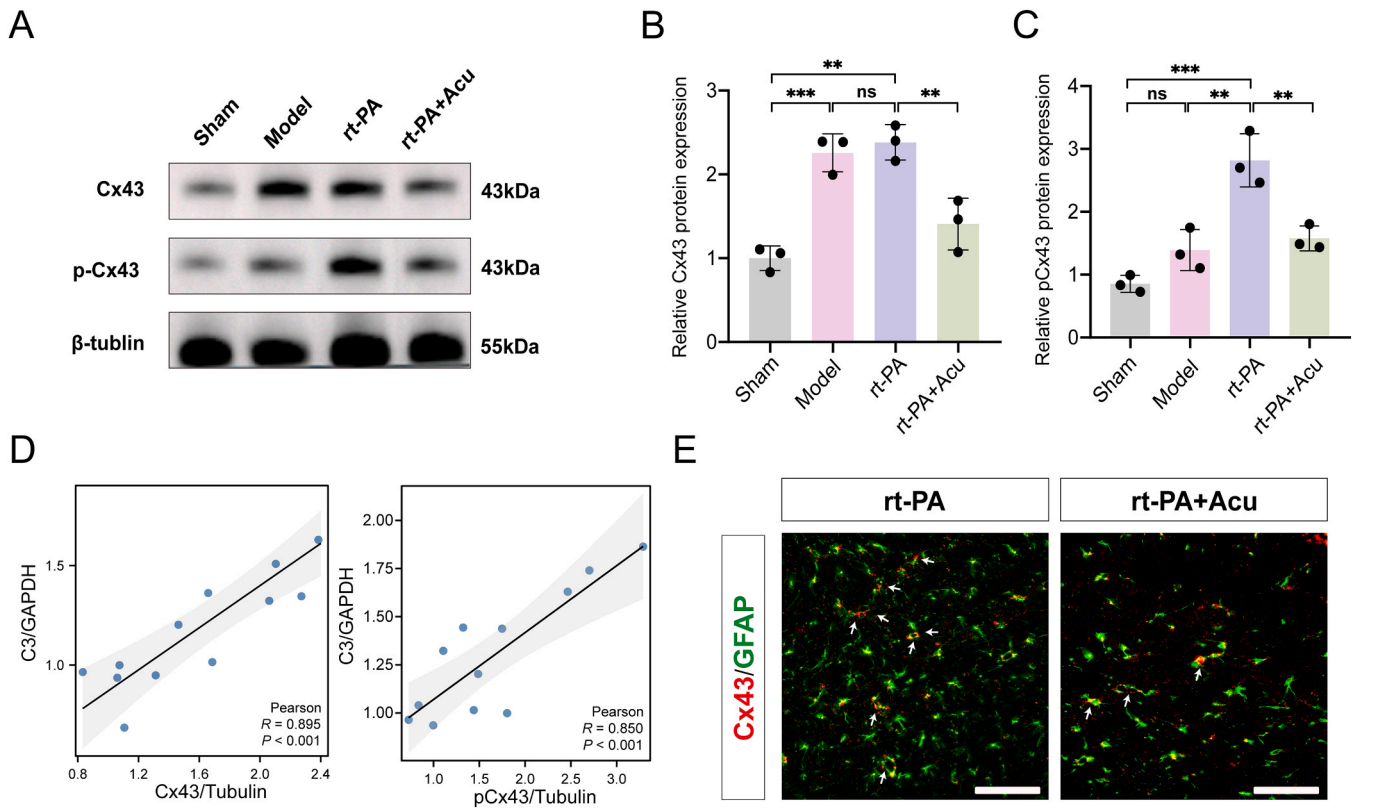

Fig. 5. Acupuncture inhibits Cx43 expression in neurotoxic astrocytes. (A) Western blot analysis of Cx43 and p-Cx43 expression in the Sham, model, rt-PA, and rt-PA+Acu groups. (B,C) Quantification of Cx43 and p-Cx43 protein expression in the western blot analysis (n = 3). (D) Correlation analysis between Cx43 and C3 expression, and p-Cx43 and C3 expression. (E) Double immunofluorescence staining for Cx43 (red) and GFAP (green) in the ischemic penumbra (Scale bar=20μm). Data was presented as mean ± SD, **p < 0.01, ***p < 0.001.

the acupuncture application as an adjunct treatment in ischemic stroke, particularly when the thrombolysis time window is delayed.

Following central nervous system injury, astrocytes undergo morphological and functional changes, a process referred to as reactive astrogliosis. In response to environmental signals, astrocytes can transition into either neurotoxic phenotype or neuroprotective phenotype (Ma et al., 2020). Various neurological diseases are accompanied by different degrees of neurotoxic/neuroprotective polarization, which highlights the potential role of astrocyte phenotypes in disease initiation and progression (Hou et al., 2020; King et al., 2020). Studies have shown that TNF-α, IL-1β, and complement component 1q (C1q), collectively known as TIC, are widely present in the peri-infarct area following stroke and induce astrocytes into the neurotoxic phenotype (Liddelow et al., 2017), and persist during the I/R phase (Hu et al., 2012). Neurotoxic reactive astrocytes lose many of their normal physiological functions, including support synapses, reuptake and recycling of glutamate, and downregulation of phagocytosis. Experiments using transgenic triple knockout mice, which cannot produce TIC cytokines, have shown that reducing astrocyte neurotoxic polarization after ischemic stroke results in smaller infarct areas and improved motor outcomes (Prescott et al., 2023).

Contrary to the previous notion that microglia were the sole mediators of neuroinflammation, astrocytes also mediated this response during brain injury and disease (Liddelow et al., 2017; Woodburn et al., 2021). Our previous studies demonstrated that acupuncture at the GV26 and PC6 acupoints alleviated the inflammatory response and inhibited astrocyte activation, and thereby mitigated BBB disruption and inhibited neuron apoptosis. This prompted us to further explore the mechanism through which acupuncture affects astrocytes. We focused on the gene regulation of astrocytes at a single level. We found that the GFAP expression in astrocytes was significantly upregulated after stroke, accompanied by neurotoxic polarization. Differential analysis revealed a significant upregulation of inflammatory cytokines, chemokines, and matrix metalloproteinases (MMPs), which is consistent with Zhang et al., who reported a significant increase in inflammatory cytokines, chemokines, MMP9, and MMP3 based on transcriptomic sequencing of in vitro neurotoxic astrocytes (Zhang et al., 2022). MMP9 and MMP3 have been reported to have detrimental effects on the integrity of the BBB. Blocking MMP9 and MMP3 significantly alleviates BBB disruption and improves neurological recovery (Turner and Sharp, 2016). Chemokines mediate inflammation and immune responses by guiding immune cell migration to the injured brain regions. For instance, CCL5 acts as a chemoattractant for T cells to inflammatory sites, mediating brain inflammation and contributing to BBB disruption (Sokol and Luster, 2015). CXCL1, produced by astrocytes, serves as a critical ligand for neutrophil transmigration across the endothelium, exacerbating brain injury (Michael et al., 2020). Additionally, studies have shown that activated MMPs degrade endothelial tight junction proteins, secrete inflammatory cytokines and adhesion molecules, and induce endothelial cell death (Rempe et al., 2016). We validated that acupuncture intervention significantly downregulated the expression of the above genes in our previously published data, caused C3 downregulation and decreased the number of $C3^{+}/GFAP^{+}$ astrocytes. This suggests that acupuncture may alleviate BBB degradation caused by neuroinflammation by inhibiting the neurotoxic polarization of reactive astrocytes.

CX43 is the primary protein that forms gap junctions between astrocytes, allowing ions and small molecules with a molecular weight below 1 kD to pass through gap junction channels. However, under pathological conditions, the aberrant opening of Cx43 hemichannels on astrocyte membranes releases small molecules into the intercellular space, which triggers cellular apoptosis and inflammatory responses.

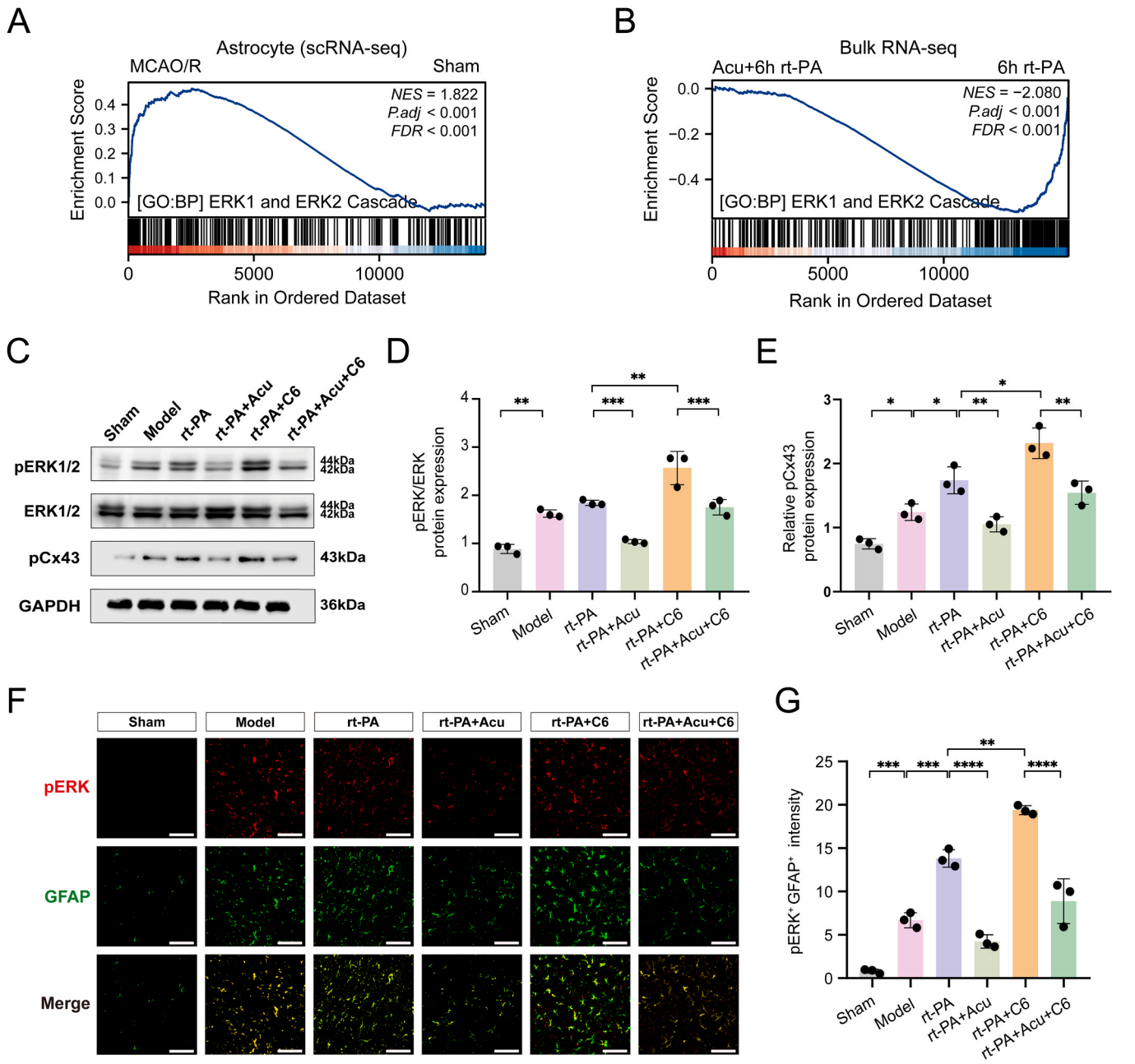

Fig. 6. Acupuncture modulates the polarization-related ERK1/2-Cx43 pathway of astrocyte. (A) Gene set enrichment analysis (GSEA) showing significant enrichment of the ERK1/2 pathway in neurotoxic polarized astrocytes. (B) GSEA showing downregulation of the ERK1/2 pathway after acupuncture intervention in delayed reperfusion. (C) Western blot analysis of p-ERK1/2 and p-Cx43 expression in the rt-PA and C6 + Acu groups. (D, E) Quantification of p-ERK1/2 and p-Cx43 protein expression from western blot analysis (n = 3). (F) Double immunofluorescence staining for p-ERK1/2 (red) and GFAP (green) in astrocytes. (G) Quantification of the intensity of $pERK^{+}/GFAP^{+}$ cells in each 1 mm^2 area of the ischemic penumbra (n = 3, Scale bar=20μm). Data was presented as mean ± SD, *p < 0.05, **p < 0.01, ***p < 0.001.

Our results revealed that acupuncture decreased the expression of CX43. After the application of the GAP19 inhibitor, the number of $GFAP^{+}$ cells significantly decreased, and the number of $C3^{+}/GFAP^{+}$ astrocytes was notably reduced. This suggests that the closure of Cx43 hemichannels may inhibit the neurotoxic polarization of reactive astrocytes. In alignment with our results, Zhao et al. observed neuronal degeneration and astrocyte dysfunction in the cadmium-induced neurotoxicity model, where astrocytes polarized to the neurotoxic state under cadmium exposure, and the internalization of Cx43 was identified as the cause of this transition (Zhao et al., 2023). Additionally, Hayato found that Cx43 knockout mice in an autoimmune encephalomyelitis model exhibited significantly downregulated neurotoxic astrocyte-related genes and C3 protein expression, which inhibited the activation of astrocytes toward a pro-inflammatory phenotype during the acute phase (Une et al., 2021). Zhao et al. also found that oligodendrocyte-specific Cx47 inhibition caused the opening of Cx43 hemichannels in astrocytes, leading to neurotoxic polarization and the activation of microglia into an inflammatory state, thereby exacerbating cerebral inflammatory responses (Zhao et al., 2020). These findings collectively suggest that astrocytes regulate inflammation through Cx43. Moreover, we found that inhibition of the hemichannel significantly reduced the expression of inflammatory cytokines IL-1β, IL-6, and TNF-α. Astrocytes are a major source of IL-6 in the central nervous system, and they also produce IFN-γ upon activation (Erta et al., 2012; Savarin et al., 2015; Xiao and Link, 1998).

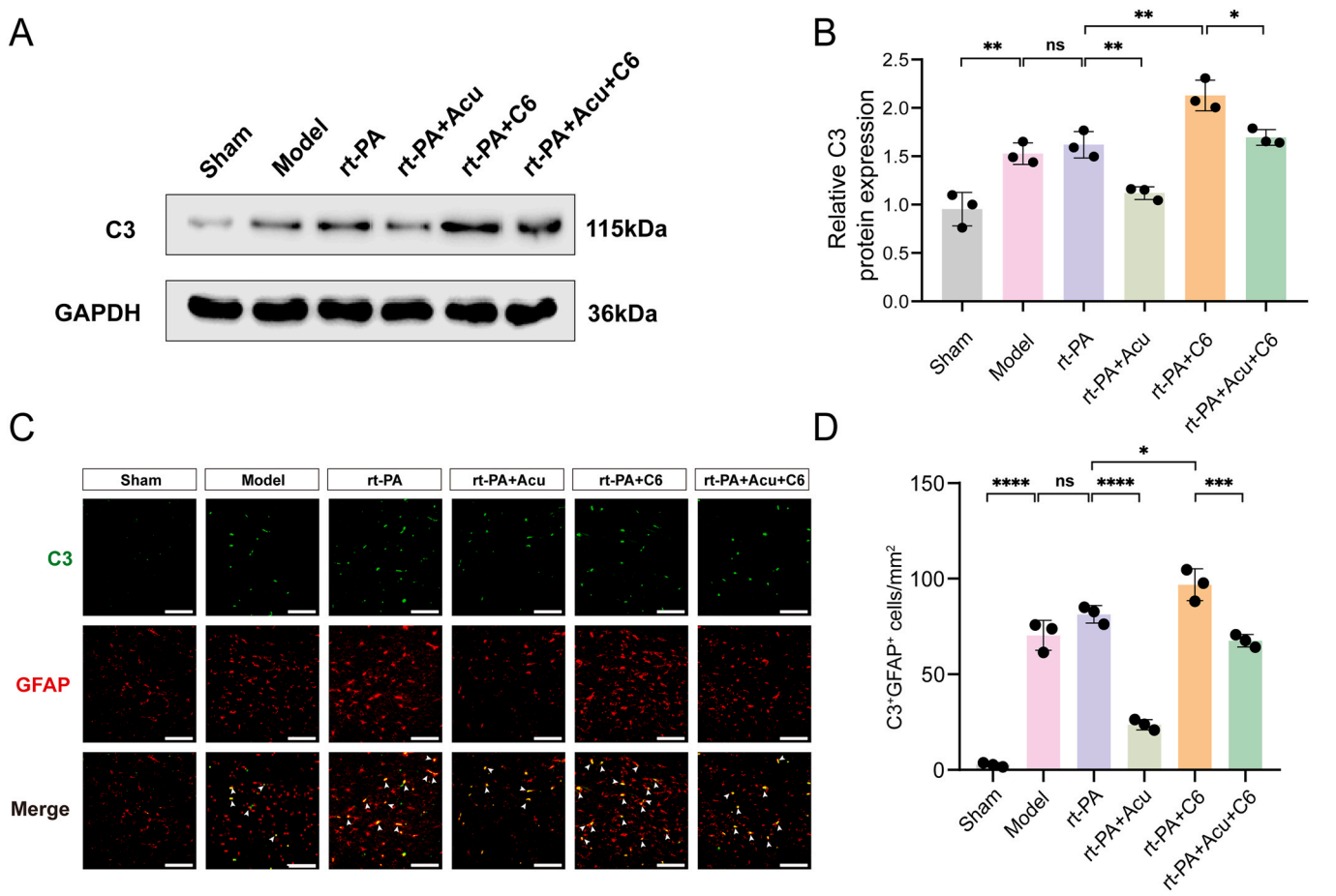

Fig. 7. Acupuncture suppresses neurotoxic polarization of astrocytes via the ERK1/2-Cx43 pathway. (a) Western blot analysis of C3 expression. (B) Quantification of p-ERK1/2 and p-Cx43 protein expression from western blot analysis (n = 3). (C) Double immunofluorescence staining for Cx43 (red) and GFAP (green). (D) Quantification of $C3^{+}/GFAP^{+}$ cells in the different groups (n = 3, Scale bar=20μm). Data was presented as mean ± SD, *p < 0.05, **p < 0.01, ***p < 0.001.

IL-6 enhances inflammation by promoting Th17 cell differentiation and increasing the accumulation of pathogenic $CD4^{+}$ T cells at the site of inflammation (Aranami and Yamamura, 2008). IFN-γ activates microglia to transition to a pro-inflammatory phenotype (Watanabe et al., 2016). The results indicate that the specific closure of astrocytic Cx43 hemichannels inhibits the neurotoxic polarization of reactive astrocytes, leading to reduced levels of cytokines and chemokines after stroke, thereby exerting a regulatory effect on post-stroke inflammation.

ERK is a member of the MAPK family, involved in signaling cascades that transmit extracellular signals to intracellular targets. Following cerebral ischemia, the ERK1/2 signaling pathway can be activated and participate in regulating processes such as inflammation, oxidative stress, and apoptosis. Specifically, activated ERK1/2 can promote the production and release of inflammatory cytokines, leading to an exacerbation of the inflammatory response. It also regulates oxidative stress, increasing the generation of free radicals and the extent of oxidative damage. Furthermore, the ERK1/2 pathway can modulate apoptotic pathways, influencing cell survival and death decisions. Currently, there is limited research on the ERK1/2 signaling pathway in astrocytes, but through GSEA analysis, we found that the ERK1/2 cascade is significantly upregulated in astrocytes following stroke, and ERK1/2 cascade is significantly downregulated following acupuncture. These findings suggest that the acupuncture intervention of the ERK1/2 cascade partially affects the neurotoxic polarization process of astrocytes. Upon the addition of ERK1/2 agonists, we observed that the phosphorylation of Cx43 is regulated by ERK1/2 phosphorylation. This is consistent with the findings of Liu et al., where the changes in Cx43 during ischemic brain injury were regulated by the ERK pathway (Liu et al., 2015). Moreover, the addition of ERK1/2 agonists significantly reversed the acupuncture-mediated inhibition of neurotoxic polarization in astrocytes, as evidenced by an increase in the expression of GFAP and C3, along with elevated levels of inflammatory cytokines such as IL-1β, IL-6, and TNF-α. Shin et al. demonstrated that after ischemic in mice, the levels of the transmembrane proteins Occludin and Claudin-5 decreased, leading to expanded tight junction gaps, along with perivascular swelling and inflammatory responses in the brain; however, these changes were reversed by the ERK1/2 signaling pathway inhibitor U0126 (Shin et al., 2015). Chen et al. found that after cerebral ischemia in rats, the phosphorylation of Cx43 in the blood-brain barrier was significantly increased (Chen et al., 2017). By using siRNA to knock down ERK1/2 or apply ERK1/2 inhibitors, the phosphorylation of Cx43 was blocked, thereby protecting the integrity of the blood-brain barrier and improving ischemic brain injury (Yang et al., 2021). These results suggest that ERK1/2, as an upstream kinase, regulates the phosphorylation of Cx43, thereby skewing astrocytes toward the neurotoxic phenotype and influencing the integrity of the blood-brain barrier.

While our study offers insights, it is not without limitations. Firstly, the embolic stroke model was used in this study, which closely mimics the pathophysiological progression of human ischemic stroke. The findings derived from this model have greater referential value, however, whether these findings can be extrapolated to humans requires further investigation. Furthermore, our study primarily focuses on the acute phase of ischemic stroke, and the long-term effects of modulating neurotoxic astrocytes remain to be investigated. Third, more studies are needed to further clarify the role of acupuncture in the regulation of neuroprotective astrocytes. Lastly, exploring other inflammation-related

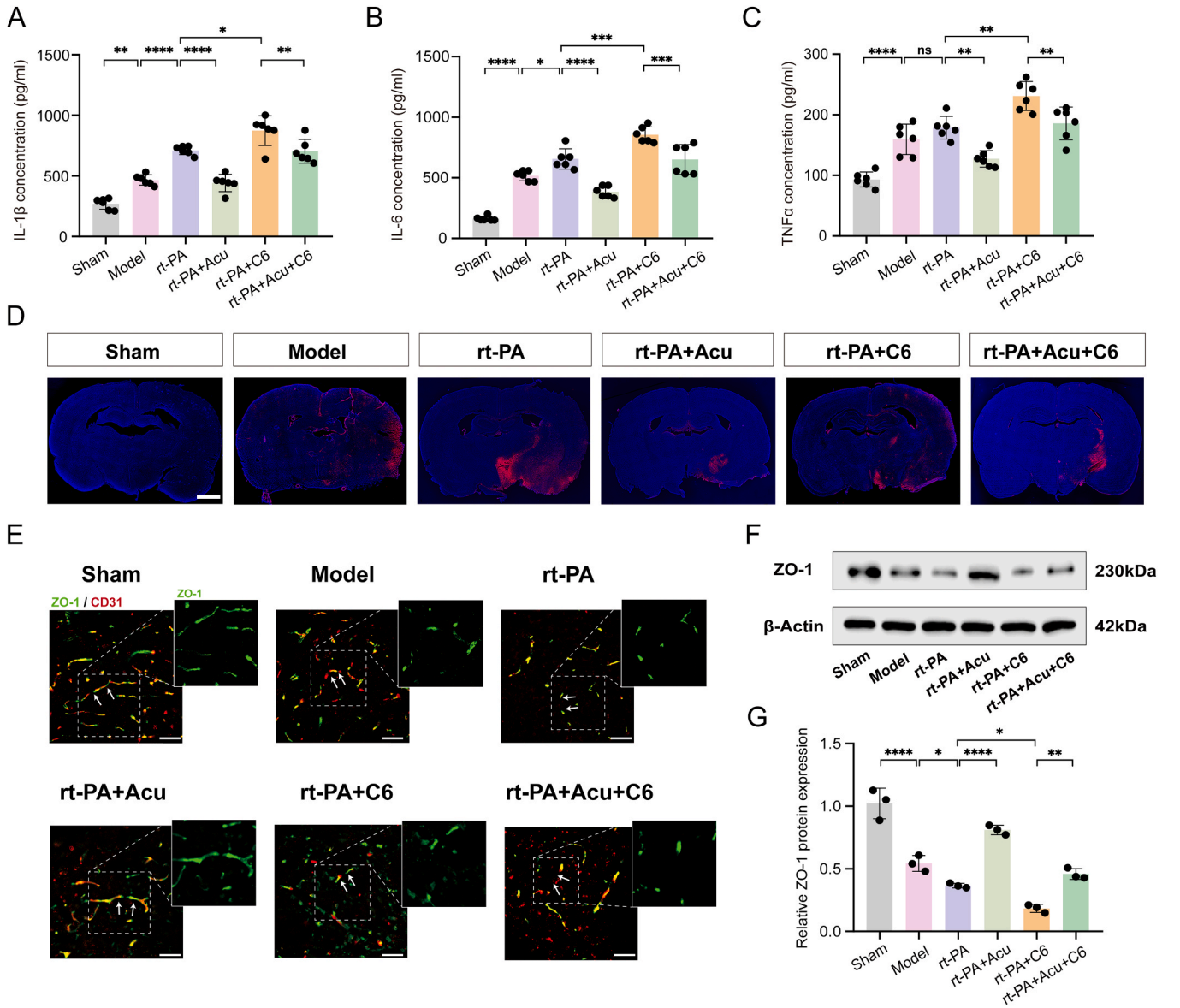

Fig. 8. Acupuncture attenuates neuroinflammation and promotes blood-brain barrier recovery via the ERK1/2/Cx43 pathway. (A-C) Concentrations of inflammatory factors IL-1β, IL-6 and TNF-α were measured across experimental groups (n = 6). (D) Representative images of BBB leakage assessed by EB fluorescence. (E) Immunofluorescence staining of tight junction protein (ZO-1, green) and endothelial cell (CD31, red) shows blood-brain barrier recovery. (F) Western blot analysis of ZO-1 expression in different groups. **(G)** Quantification of ZO-1 protein expression from Western blot analysis (n = 3). Data was presented as mean ± SD, *p < 0.05, **p < 0.01, ***p < 0.001.

components involved in acupuncture -mediated immune modulation could provide a more comprehensive understanding of its role in stroke pathology.

In conclusion, this study elucidates the mechanisms by which acupuncture promotes neuroprotection following delayed thrombolysis. Acupuncture modulates the ERK1/2-Cx43 signaling pathway to regulate neurotoxic astrocyte-mediated inflammation and preserve blood-brain barrier integrity, thereby mitigating brain injury. These results offer novel insights into astrocyte polarization and highlight acupuncture as a potential therapeutic strategy for stroke.

Ethics statement

The Institutional Animal Care and Use Committee of Nanjing University of Chinese Medicine (Approval No. 202312A034) approved the animal experiments conducted in this study, which were strictly in accordance with the guidelines established by the National Institutes of Health Animal Care and Use Committee.

Funding

This research was funded by National Natural Science Foundation of China (grant number. 82274639).

CRediT authorship contribution statement

Ni GuangXia: Conceptualization, Methodology, Supervision. **Gu Yu:** Data curation, Formal analysis, Writing – original draft, Writing – review & editing. **Zhang ZhiHui:** Data curation, Formal analysis, Writing – original draft, Writing – review & editing. **Liu XinYu:** Writing – review & editing. **Huang Zheng:** Writing – review & editing. **Zhang XinChang:** Writing – review & editing. **Xu WenTao:** Writing – review & editing.

Declaration of Competing Interest

The authors declare that they have no known competing financial interests or personal relationships that could have appeared to influence the work reported in this paper.

Appendix A. Supporting information

Supplementary data associated with this article can be found in the online version at doi:10.1016/j.ibneur.2025.04.005.

References

Almad, A.A., Taga, A., Joseph, J., Gross, S.K., Welsh, C., Patankar, A., Richard, J.P., Rust, K., Pokharel, A., Plott, C., et al., 2022. Cx43 hemichannels contribute to astrocyte-mediated toxicity in sporadic and familial ALS. Proc. Natl. Acad. Sci. USA 119, e2107391119. https://doi.org/10.1073/pnas.2107391119.

Andreatta, M., Carmona, S.J., 2021. UCell: robust and scalable single-cell gene signature scoring. Comput. Struct. Biotechnol. J. 19, 3796–3798. https://doi.org/10.1016/j.csbj.2021.06.043.

Aranami, T., Yamamura, T., 2008. Th17 Cells and autoimmune encephalomyelitis (EAE/MS). Allergol. Int. 57, 115–120. https://doi.org/10.2332/allergolint.R-07-159.

Bhuva, D.D., Foroutan, M., Xie, Y., Lyu, R., Cursons, J., Davis, M.J., 2019. Using singscore to predict mutation status in acute myeloid leukemia from transcriptomic signatures. F1000Res. 8, 776. https://doi.org/10.12688/f1000research.19236.3.

Bormann, D., Knoflach, M., Poreba, E., Riedl, C.J., Testa, G., Orset, C., Levilly, A., Cottereau, A., Jauk, P., Hametner, S., et al., 2024. Single-nucleus RNA sequencing reveals glial cell type-specific responses to ischemic stroke in male rodents. Nat. Commun. 15, 6232. https://doi.org/10.1038/s41467-024-50465-z.

Bush, T.G., Puvanachandra, N., Horner, C.H., Polito, A., Ostenfeld, T., Svendsen, C.N., Mucke, L., Johnson, M.H., Sofroniew, M.V., 1999. Leukocyte infiltration, neuronal degeneration, and neurite outgrowth after ablation of scar-forming, reactive astrocytes in adult transgenic mice. Neuron 23, 297–308. https://doi.org/10.1016/s0896-6273(00)80781-3.

Campbell, B.C.V., De Silva, D.A., Macleod, M.R., Coutts, S.B., Schwamm, L.H., Davis, S.M., Donnan, G.A., 2019. Ischaemic stroke. Nat. Rev. Dis. Prim. 5, 70. https://doi.org/10.1038/s41572-019-0118-8.

Chen, W., Feng, J., Tong, W., 2017. Phosphorylation of astrocytic connexin43 by ERK1/2 impairs blood-brain barrier in acute cerebral ischemia. Cell Biosci. 7, 43. https://doi.org/10.1186/s13578-017-0170-6.

Chen, Z., Li, T., Tang, H.B., Lu, Z.W., Chen, Z.Y., Zhao, Z.H., Yang, X.L., Zhao, L.L., Dang, M.J., Li, Y., et al., 2024a. Edaravone Dexborneol provides neuroprotective effect by inhibiting neurotoxic activation of astrocytes through inhibiting NF-kappaB signaling in cortical ischemia. Brain Res. Bull. 218, 111097. https://doi.org/10.1016/j.brainresbull.2024.111097.

Chen, X., Wang, W., Li, H., Zhang, X., 2023. Enriched environment alleviates neurological deficits via downregulation of Cx43 after experimental stroke. Brain Res. 1821, 148619. https://doi.org/10.1016/j.brainres.2023.148619.

Chen, W., Wu, Z., Yin, M., Zhang, Y., Qin, Y., Liu, X., Tu, J., 2024b. Blockage of p38MAPK in astrocytes alleviates brain damage in a mouse model of embolic stroke through the CX43/AQP4 axis. J. Stroke Cereb. Dis. 33, 108085. https://doi.org/10.1016/j.jstrokecerebrovasdis.2024.108085.

China Association of Acupuncture and Moxibustion, 2021. Names and Locations of Commonly Used Acupoints in Laboratory Animals - Part 2: Rats. Acupuncture research, 46, 351-352..

Erta, M., Quintana, A., Hidalgo, J., 2012. Interleukin-6, a major cytokine in the central nervous system. Int. J. Biol. Sci. 8, 1254–1266. https://doi.org/10.7150/ijbs.4679.

Fan, Y.Y., Huo, J., 2021. A1/A2 astrocytes in central nervous system injuries and diseases: Angels or devils? Neurochem. Int. 148, 105080. https://doi.org/10.1016/j.neuint.2021.105080.

Hao, Y., Hao, S., Andersen-Nissen, E., Mauck 3rd, W.M., Zheng, S., Butler, A., Lee, M.J., Wilk, A.J., Darby, C., Zager, M., et al., 2021. Integrated analysis of multimodal single-cell data. e3529 Cell 184, 3573–3587. https://doi.org/10.1016/j.cell.2021.04.048.

Herpich, F., Rincon, F., 2020. Management of acute ischemic stroke. Crit. Care Med. 48, 1654–1663. https://doi.org/10.1097/CCM.0000000000004597.

Hou, B., Zhang, Y., Liang, P., He, Y., Peng, B., Liu, W., Han, S., Yin, J., He, X., 2020. Inhibition of the NLRP3-inflammasome prevents cognitive deficits in experimental autoimmune encephalomyelitis mice via the alteration of astrocyte phenotype. Cell death Dis. 11, 377. https://doi.org/10.1038/s41419-020-2565-2.

Hu, X., Li, P., Guo, Y., Wang, H., Leak, R.K., Chen, S., Gao, Y., Chen, J., 2012. Microglia/macrophage polarization dynamics reveal novel mechanism of injury expansion after focal cerebral ischemia. Stroke 43, 3063–3070. https://doi.org/10.1161/STROKEAHA.112.659656.

Jin, Y., Wang, Z., He, D., Zhu, Y., Chen, X., Cao, K., 2021. Identification of novel subtypes based on ssGSEA in immune-related prognostic signature for tongue squamous cell carcinoma. Cancer Med. 10, 8693–8707. https://doi.org/10.1002/cam4.4341.

Jurcau, A., Simion, A., 2021. Neuroinflammation in cerebral ischemia and ischemia/reperfusion injuries: from pathophysiology to therapeutic strategies. Int. J. Mol. Sci. 23. https://doi.org/10.3390/ijms23010014.

King, A., Szekely, B., Calapkulu, E., Ali, H., Rios, F., Jones, S., Troakes, C., 2020. The increased densities, but different distributions, of both C3 and S100A10 immunopositive astrocyte-like cells in alzheimer's disease brains suggest possible roles for both A1 and A2 astrocytes in the disease pathogenesis. Brain Sci. 10. https://doi.org/10.3390/brainsci10080503.

Lee, H.G., Wheeler, M.A., Quintana, F.J., 2022. Function and therapeutic value of astrocytes in neurological diseases. Nat. Rev. Drug Discov. 21, 339–358. https://doi.org/10.1038/s41573-022-00390-x.

Lei, Y., Peng, X., Li, T., Liu, L., Yang, G., 2019. ERK and miRNA-1 target Cx43 expression and phosphorylation to modulate the vascular protective effect of angiotensin II. Life Sci. 216, 59–66. https://doi.org/10.1016/j.lfs.2018.11.019.

Liang, Z., Wang, X., Hao, Y., Qiu, L., Lou, Y., Zhang, Y., Ma, D., Feng, J., 2020. The multifaceted role of astrocyte connexin 43 in ischemic stroke through forming hemichannels and gap junctions. Front. Neurol. 11, 703. https://doi.org/10.3389/fneur.2020.00703.

Liddelow, S.A., Barres, B.A., 2017. Reactive astrocytes: production, function, and therapeutic potential. Immunity 46, 957–967. https://doi.org/10.1016/j.immuni.2017.06.006.

Liddelow, S.A., Guttenplan, K.A., Clarke, L.E., Bennett, F.C., Bohlen, C.J., Schirmer, L., Bennett, M.L., Munch, A.E., Chung, W.S., Peterson, T.C., et al., 2017. Neurotoxic reactive astrocytes are induced by activated microglia. Nature 541, 481–487. https://doi.org/10.1038/nature21029.

Liu, L., Li, C.J., Lu, Y., Zong, X.G., Luo, C., Sun, J., Guo, L.J., 2015. Baclofen mediates neuroprotection on hippocampal CA1 pyramidal cells through the regulation of autophagy under chronic cerebral hypoperfusion. Sci. Rep. 5, 14474. https://doi.org/10.1038/srep14474.

Liu, Y., Li, H., Zeng, T., Wang, Y., Zhang, H., Wan, Y., Shi, Z., Cao, R., Tang, H., 2023. Integrated bulk and single-cell transcriptomes reveal pyroptotic signature in prognosis and therapeutic options of hepatocellular carcinoma by combining deep learning. Brief. Bioinformatics 25. https://doi.org/10.1093/bib/bbad487.

Liu, H., Shen, Y., Huang, Z., Jiang, T., Huang, P., Yang, M., Zhang, X., Xu, W., Ni, G., 2024. Electroacupuncture extends the time window of thrombolytic therapy in rats by reducing disruptions of blood-brain barrier and inhibiting GSDMD-mediated pyroptosis. Brain Res. 1845, 149296. https://doi.org/10.1016/j.brainres.2024.149296.

Love, M.I., Huber, W., Anders, S., 2014. Moderated estimation of fold change and dispersion for RNA-seq data with DESeq2. Genome Biol. 15, 550. https://doi.org/10.1186/s13059-014-0550-8.

Ma, M., Li, H., Wu, J., Zhang, Y., Shen, H., Li, X., Wang, Z., Chen, G., 2020. Roles of prokineticin 2 in subarachnoid hemorrhage-induced early brain injury via regulation of phenotype polarization in astrocytes. Mol. Neurobiol. 57, 3744–3758. https://doi.org/10.1007/s12035-020-01990-7.

Mei, Y., Li, M., Wen, J., Kong, X., Li, J., 2023. Single-cell characteristics and malignancy regulation of alpha-fetoprotein-producing gastric cancer. Cancer Med. 12, 12018–12033. https://doi.org/10.1002/cam4.5883.

Mendelson, S.J., Prabhakaran, S., 2021. Diagnosis and management of transient ischemic attack and acute ischemic stroke: a review. JAMA 325, 1088–1098. https://doi.org/10.1001/jama.2020.26867.

Michael, B.D., Bricio-Moreno, L., Sorensen, E.W., Miyabe, Y., Lian, J., Solomon, T., Kurt-Jones, E.A., Luster, A.D., 2020. Astrocyte- and neuron-derived CXCL1 drives neutrophil transmigration and blood-brain barrier permeability in viral encephalitis. Cell Rep. 32, 108150. https://doi.org/10.1016/j.celrep.2020.108150.

Moorer, M.C., Stains, J.P., 2017. Connexin43 and the intercellular signaling network regulating skeletal remodeling. Curr. Osteoporos. Rep. 15, 24–31. https://doi.org/10.1007/s11914-017-0345-4.

Ohashi, S.N., DeLong, J.H., Kozberg, M.G., Mazur-Hart, D.J., van Veluw, S.J., Alkayed, N.J., Sansing, L.H., 2023. Role of inflammatory processes in hemorrhagic stroke. Stroke 54, 605–619. https://doi.org/10.1161/STROKEAHA.122.037155.

Prescott, K., Munch, A.E., Brahms, E., Weigel, M.K., Inoue, K., Buckwalter, M.S., Liddelow, S.A., Peterson, T.C., 2023. Blocking of microglia-astrocyte proinflammatory signaling is beneficial following stroke. Front. Mol. Neurosci. 16, 1305949. https://doi.org/10.3389/fnmol.2023.1305949.

Qin, S., Zhang, Z., Zhao, Y., Liu, J., Qiu, J., Gong, Y., Fan, W., Guo, Y., Guo, Y., Xu, Z., et al., 2022. The impact of acupuncture on neuroplasticity after ischemic stroke: a literature review and perspectives. Front. Cell Neurosci. 16, 817732. https://doi.org/10.3389/fncel.2022.817732.

Rempe, R.G., Hartz, A.M.S., Bauer, B., 2016. Matrix metalloproteinases in the brain and blood-brain barrier: versatile breakers and makers. J. Cereb. Blood Flow. Metab. 36, 1481–1507. https://doi.org/10.1177/0271678X16655551.

Revuelta, M., Elicegui, A., Moreno-Cugnon, L., Buhrer, C., Matheu, A., Schmitz, T., 2019. Ischemic stroke in neonatal and adult astrocytes. Mech. Ageing Dev. 183, 111147. https://doi.org/10.1016/j.mad.2019.111147.

Savarin, C., Hinton, D.R., Valentin-Torres, A., Chen, Z., Trapp, B.D., Bergmann, C.C., Stohlman, S.A., 2015. Astrocyte response to IFN-gamma limits IL-6-mediated microglia activation and progressive autoimmune encephalomyelitis. J. Neuroinflamm. 12, 79. https://doi.org/10.1186/s12974-015-0293-9.

Shaul, Y.D., Seger, R., 2007. The MEK/ERK cascade: from signaling specificity to diverse functions. Biochim Biophys. Acta 1773, 1213–1226. https://doi.org/10.1016/j.bbamcr.2006.10.005.

Shin, J.A., Kim, Y.A., Jeong, S.I., Lee, K.E., Kim, H.S., Park, E.M., 2015. Extracellular signal-regulated kinase1/2-dependent changes in tight junctions after ischemic preconditioning contributes to tolerance induction after ischemic stroke. Brain Struct. Funct. 220, 13–26. https://doi.org/10.1007/s00429-013-0632-5.

Sokol, C.L., Luster, A.D., 2015. The chemokine system in innate immunity. Cold Spring Harb. Perspect. Biol. 7. https://doi.org/10.1101/cshperspect.a016303.

Subramanian, A., Tamayo, P., Mootha, V.K., Mukherjee, S., Ebert, B.L., Gillette, M.A., Paulovich, A., Pomeroy, S.L., Golub, T.R., Lander, E.S., et al., 2005. Gene set enrichment analysis: a knowledge-based approach for interpreting genome-wide

expression profiles. Proc. Natl. Acad. Sci. USA 102, 15545–15550. https://doi.org/10.1073/pnas.0506580102.

Tsivgoulis, G., Katsanos, A.H., Sandset, E.C., Turc, G., Nguyen, T.N., Bivard, A., Fischer, U., Khatri, P., 2023. Thrombolysis for acute ischaemic stroke: current status and future perspectives. Lancet Neurol. 22, 418–429. https://doi.org/10.1016/S1474-4422(22)00519-1.

Turner, R.J., Sharp, F.R., 2016. Implications of MMP9 for blood brain barrier disruption and hemorrhagic transformation following ischemic stroke. Front. Cell Neurosci. 10, 56. https://doi.org/10.3389/fncel.2016.00056.

Une, H., Yamasaki, R., Nagata, S., Yamaguchi, H., Nakamuta, Y., Indiasari, U.C., Cui, Y., Shinoda, K., Masaki, K., Gotz, M., et al., 2021. Brain gray matter astroglia-specific connexin 43 ablation attenuates spinal cord inflammatory demyelination. J. Neuroinflamm. 18, 126. https://doi.org/10.1186/s12974-021-02176-1.

Wang, S., Pan, Y., Zhang, C., Zhao, Y., Wang, H., Ma, H., Sun, J., Zhang, S., Yao, J., Xie, D., et al., 2024. Transcriptome analysis reveals dynamic microglial-induced A1 astrocyte reactivity via C3/C3aR/NF-kappaB signaling after ischemic stroke. Mol. Neurobiol. 61, 10246–10270. https://doi.org/10.1007/s12035-024-04210-8.

Watanabe, M., Masaki, K., Yamasaki, R., Kawanokuchi, J., Takeuchi, H., Matsushita, T., Suzumura, A., Kira, J.I., 2016. Th1 cells downregulate connexin 43 gap junctions in astrocytes via microglial activation. Sci. Rep. 6, 38387. https://doi.org/10.1038/srep38387.

Woodburn, S.C., Bollinger, J.L., Wohleb, E.S., 2021. The semantics of microglia activation: neuroinflammation, homeostasis, and stress. J. Neuroinflamm. 18, 258. https://doi.org/10.1186/s12974-021-02309-6.

Wu, T., Hu, E., Xu, S., Chen, M., Guo, P., Dai, Z., Feng, T., Zhou, L., Tang, W., Zhan, L., et al., 2021. clusterProfiler 4.0: a universal enrichment tool for interpreting omics data. Innovation 2, 100141. https://doi.org/10.1016/j.xinn.2021.100141.

Xiao, B.G., Link, H., 1998. IFN-gamma production of adult rat astrocytes triggered by TNF-alpha. Neuroreport 9, 1487–1490. https://doi.org/10.1097/00001756-199805110-00044.

Xu, W.T., Jiang, S.Y., Chang, S.Q., Zhang, Z.H., Song, Y.Y., Zhang, X.C., Ni, G.X., 2021. Experimental study on the safety of hypertime window thrombolysis for cerebral infarction by inhibiting the activation of astrocytes with acupuncture. J. Nanjing Univ. Tradit. Chin. Med. 37, 685–695. https://doi.org/10.14148/j.issn.1672-0482.2021.0688.

Yang, Z.X., Xie, J.H., Liu, D.D., 2017. Xingnao Kaiqiao needling method for acute ischemic stroke: a meta-analysis of safety and efficacy. Neural Regen. Res. 12, 1308–1314. https://doi.org/10.4103/1673-5374.213551.

Yang, Z.X., Xie, J.H., Liu, Y.P., Miao, G.X., Wang, Y.H., Wu, S.M., Li, Y., 2015. Systematic review of long-term Xingnao Kaiqiao needling effcacy in ischemic stroke treatment. Neural Regen. Res. 10, 583–588. https://doi.org/10.4103/1673-5374.155431.

Yang, Y., Yang, L.Y., Salayandia, V.M., Thompson, J.F., Torbey, M., Yang, Y., 2021. Treatment with atorvastatin during vascular remodeling promotes pericyte-mediated blood-brain barrier maturation following ischemic stroke. Transl. Stroke Res. 12, 905–922. https://doi.org/10.1007/s12975-020-00883-0.

Zhang, X.-c, Gu, Y.-h, Xu, W.-t, Song, Y.-y, Zhang, A., Zhang, Z.-h, Jiang, S.-y, Chang, S.-q, Ni, G.-x, 2020. Early electroacupuncture extends the rtPA Time Window to 6h in a male rat model of embolic stroke via the ERK1/2-MMP9 pathway. Neural Plast., 8851089 https://doi.org/10.1155/2020/8851089.

Zhang, Q., Liu, C., Shi, R., Zhou, S., Shan, H., Deng, L., Chen, T., Guo, Y., Zhang, Z., Yang, G.Y., et al., 2022. Blocking C3d(+)/GFAP(+) A1 astrocyte conversion with semaglutide attenuates blood-brain barrier disruption in mice after ischemic stroke. Aging Dis. 13, 943–959. https://doi.org/10.14336/ad.2021.1029.

Zhang, Z., Lu, T., Li, S., Zhao, R., Li, H., Zhang, X., Li, Y., Xia, Y., Ni, G., 2024b. Acupuncture extended the thrombolysis window by suppressing blood-brain barrier disruption and regulating autophagy-apoptosis balance after ischemic stroke. Brain Sci. 14. https://doi.org/10.3390/brainsci14040399.

Zhang, S., Shang, D., Shi, H., Teng, W., Tian, L., 2021. Function of astrocytes in neuroprotection and repair after ischemic stroke. Eur. Neurol. 84, 426–434. https://doi.org/10.1159/000517378.

Zhang, L., Zhang, R.L., Jiang, Q., Ding, G., Chopp, M., Zhang, Z.G., 2015. Focal embolic cerebral ischemia in the rat. Nat. Protoc. 10, 539–547. https://doi.org/10.1038/nprot.2015.036.

Zhang, L., Zhao, G., Luo, Z., Yu, Z., Liu, G., Su, G., Tang, X., Yuan, Z., Huang, C., Sun, H. S., et al., 2024a. AD16 attenuates neuroinflammation induced by cerebral ischemia through down-regulating astrocytes A1 polarization. Biomed. Pharm. 178, 117209. https://doi.org/10.1016/j.biopha.2024.117209.

Zhao, Y.X., Li, X.N., Tang, Y.X., Talukder, M., Zhao, Y., Li, J.L., 2023. Cadmium transforms astrocytes into the A1 subtype via inducing gap junction protein connexin 43 into the nucleus. J. Agric. Food Chem. 71, 12043–12051. https://doi.org/10.1021/acs.jafc.3c02963.

Zhao, Y., Yamasaki, R., Yamaguchi, H., Nagata, S., Une, H., Cui, Y., Masaki, K., Nakamuta, Y., Iinuma, K., Watanabe, M., et al., 2020. Oligodendroglial connexin 47 regulates neuroinflammation upon autoimmune demyelination in a novel mouse model of multiple sclerosis. Proc. Natl. Acad. Sci. USA 117, 2160–2169. https://doi.org/10.1073/pnas.1901294117.

Zheng, K., Lin, L., Jiang, W., Chen, L., Zhang, X., Zhang, Q., Ren, Y., Hao, J., 2022. Single-cell RNA-seq reveals the transcriptional landscape in ischemic stroke. J. Cereb. Blood Flow. Metab. 42, 56–73. https://doi.org/10.1177/0271678X211026770.